AD-A085 102 PENNSYLVANIA STATE UNIV UNIVERSITY PARK APPLIED RESE--ETC F/G 20/4
A WATER MODEL STUDY OF RECIRCULATING FLOW IN A SINGLE INJECTOR --ETC(U)
APR 80 S LAL, C H WOLGEMUTH N00024-79-C-6043
UNCLASSIFIED ARL/PSU/TM-80-46 NL

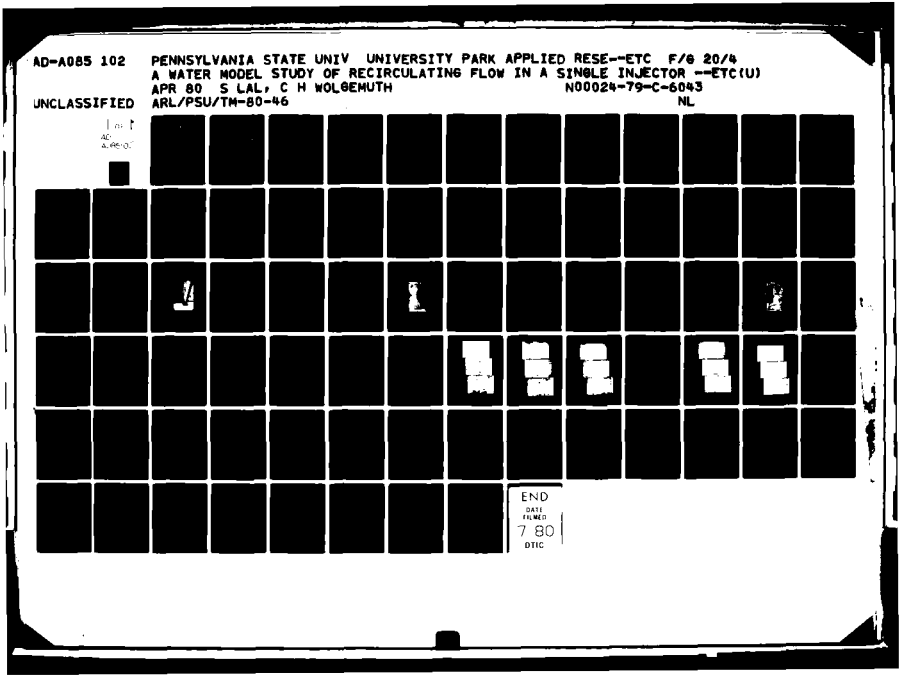

LEVEL II

12

A WATER MODEL STUDY OF RECIRCULATING FLOW IN A SINGLE INJECTOR REACTOR

Shyam Lal and Carl H. Wolgemuth

Technical Memorandum
File No. TM 80-46
April 1, 1980
Contract No. N00024-79-C-6043

Copy No. 8

The Pennsylvania State University
Institute for Science and Engineering
APPLIED RESEARCH LABORATORY
P. O. Box 30
State College, PA 16801

NAVY DEPARTMENT

NAVAL SEA SYSTEMS COMMAND

UNCLASSIFIED

SECURITY CLASSIFICATION OF THIS PAGE (When Data Entered)

REPORT DOCUMENTATION PAGE	READ INSTRUCTIONS BEFORE COMPLETING FORM
1. REPORT NUMBER: (14) ARL/PSU/TM-80-46 / 2. GOVT ACCESSION NO.: AD-A085102	3. RECIPIENT'S CATALOG NUMBER
4. TITLE (and Subtitle): (6) A WATER MODEL STUDY OF RECIRCULATING FLOW IN A SINGLE INJECTOR REACTOR.	5. TYPE OF REPORT & PERIOD COVERED: (9) Technical Memorandum 6. PERFORMING ORG. REPORT NUMBER
7. AUTHOR(s): (10) Shyam Lal and Carl H. Wolgemuth	8. CONTRACT OR GRANT NUMBER(s): (15) N00024-79-C-6043
9. PERFORMING ORGANIZATION NAME AND ADDRESS: APPLIED RESEARCH LABORATORY, P. O. BOX 30, STATE COLLEGE, PA 16801	10. PROGRAM ELEMENT, PROJECT, TASK AREA & WORK UNIT NUMBERS: 12 761
11. CONTROLLING OFFICE NAME AND ADDRESS: NAVAL SEA SYSTEMS COMMAND (SEA 63R-32), DEPARTMENT OF THE NAVY, WASHINGTON, DC 20360	(11) 12. REPORT DATE: 1 Apr 80 13. NUMBER OF PAGES: 72
14. MONITORING AGENCY NAME & ADDRESS (if different from Controlling Office)	15. SECURITY CLASS. (of this report): UNCLASSIFIED 15a. DECLASSIFICATION DOWNGRADING SCHEDULE

16. DISTRIBUTION STATEMENT (of this Report)

Approved for Public Release. Distribution Unlimited.

Per NAVSEA - May 12, 1980.

17. DISTRIBUTION STATEMENT (of the abstract entered in Block 20, if different from Report)

18. SUPPLEMENTARY NOTES

19. KEY WORDS (Continue on reverse side if necessary and identify by block number)

flow, field, visualization, water, cylinder

20. ABSTRACT (Continue on reverse side if necessary and identify by block number)

A cylindrical water model was used to visualize the flow field in a jet-stirred bath. The model was made of transparent plexiglass. A plane of light illuminated a cross section of the cylinder containing its axis and the point of injection; and thereby illuminating the small alumina particles suspended in the water. The flow field was photographed, and dye visualization studies were also conducted.

A simple modification to the TEACH computer code was made so as to account

DD FORM 1 JAN 73 1473 EDITION OF 1 NOV 65 IS OBSOLETE

UNCLASSIFIED 371

SECURITY CLASSIFICATION OF THIS PAGE (When Data Entered)

20. ABSTRACT (Cont'd)

for the geometry of the model. Computer runs were made for different injector Reynolds numbers.

Conclusions were made regarding the mean and fluctuating nature of the flow field.

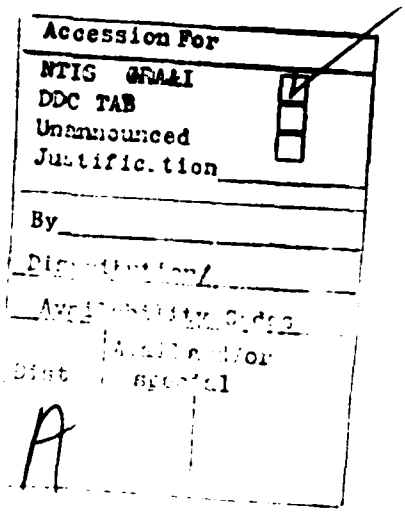

Subject: A Water Model Study of Recirculating Flow in a Single Injector Reactor

Abstract:

A cylindrical water model was used to visualize the flow field in a jet-stirred bath. The model was made of transparent plexiglass. A plane of light illuminated a cross section of the cylinder containing its axis and the point of injection; and thereby illuminating the small alumina particles suspended in the water. The flow field was photographed, and dye visualization studies were also conducted.

A simple modification to the TEACH computer code was made so as to account for the geometry of the model. Computer runs were made for different injector Reynolds numbers.

Conclusions were made regarding the mean and fluctuating nature of the flow field.

TABLE OF CONTENTS

LIST OF TABLES

LIST OF FIGURES

NOMENCLATURE

Symbol	
A_E	coefficient of finite difference equation
Ct	Craya-Curtet Number
d	injector diameter
D	cylinder diameter
j_e	flux (defined in Appendix A)
k	turbulent kinetic energy
P	pressure
U	axial velocity
$\overline{U}_{in}$	mean injector velocity
V	radial velocity
Δx	axial grid spacing
ρ	density
ε	turbulence energy dissipation rate
ϕ	any variable (e.g. k,U,V)
Γ_ϕ	exchange coefficient of ϕ

CHAPTER I

INTRODUCTION

1.1 Statement of the Problem

This study is aimed at obtaining an understanding of the recirculating flow field in a modified single injector reactor (SIR). This consisted of an injector stirred liquid bath in a cylinder modified to have outflow on both ends. The primary objective is to qualitatively obtain a picture of the flow structure as a function of the injector Reynolds number and the ratio of outflow at the two ends of the model.

1.2 Origin and Relevance of the Study

The flow field and heat transfer characteristics of a jet stirred bath are of significant interest. Such a jet mixing process is employed in many combustion applications. An example of such a system is a boiler reactor. In this case, the fuel is a molten Lithium bath and the oxidizer is injected into the reactor. The reaction is exothermic, and the resulting heat generated is transferred to a boiler which provides steam to the power cycle. The jet induced mixing causes an augmented heat transfer rate to the water.

Work has been done to obtain empirical relationships for the heat transfer coefficients (1), and to develop analytic models for the velocity distribution and heat transfer coefficients. However, it was felt that in order to develop suitable predictor techniques for such situations, a more fundamental understanding of the flow structure is essential.

1.3 Previous Related Studies

Mixing in ducted turbulent jets was examined by Becker, Hottel and Williams (2). They studied the effect of the Craya-Curtet similarity parameter on turbulent mixing patterns in axisymmetric, constant density confined jet flows, in the regime in which recirculation occurred. Their experimental set-up consisted of a round jet discharging axially into a cylindrical duct fed by a uniform stream whose entrance momentum relative to that of the jet varied from zero to moderately high values. The fields of mean velocity and mean concentration were mapped and analyzed. They concluded that at small values of the Craya-Curtet number (Ct), the initial stream flow into the duct falls short of the entrainment needed by the jet. The deficiency is made up by fluid recirculated from downstream. They describe properties of the recirculation eddy and the post jet mixing zone downstream of reattachment. It should be noted that in the SIR the initial stream velocity is zero and Ct approaches zero implying total recirculation.

Barchilon and Curtet (3) in attempting to improve the assumptions made in the approximate theory of confined jets (4,5,6) made some interesting visualization studies. They detected unusually high turbulence levels in the jet and recirculation regions. They found that the recirculation eddy which initially appeared at a Craya-Curtet number of 0.976 extended itself as Ct diminished and at Ct = 0.075 it occupied the complete duct. Low Craya-Curtet numbers are indicative of high turbulence and large eddies implying better mixing. There have been many

other studies on recirculating flows in ducted jets, they have been well summarized in (1), (2) and (3).

Abramovich (7) developed a theory for predicting flow patterns in a dead ended channel stirred by a submerged injector, which is the situation existing in the SIR. Abramovich treated the flow region as two separate parts; the first in which the turbulent jet spreads through a counterflowing stream of fluid, and the second in which the streamlines turn in accordance with the laws of motion of an ideal fluid. Solutions for the velocity fields were obtained by solving the conservation equations in each area. Only incompressible fluids were considered and corrections were applied to these solutions to account for non-uniform exit velocity profile. Comparison with experimental results showed good agreement of the prediction in the first region but very poor prediction in the second region.

Some preliminary work at ARL analytically determined the velocity distribution and the wall heat transfer coefficient for a closed ended cylinder similar to the SIR. The model divides the flow field into four parts: (i) Jet with core region, (ii) Developing or spreading jet region, (iii) Viscous dissipation region, and (iv) Stagnation region. The analysis employs previous free jet (8) and open ended confined jets (7,9) to develop equations which are solved numerically. A closed end effect is generated by incorporating a stagnation region. The fluid was assumed to be incompressible and both local and overall heat transfer calculations made. No comparison to experimental data was made.

Kerney, et al. (10) and Weimer, et al. (11) studied the penetration characteristics of vapor jets submerged in subcooled baths. Experimental results were used to develop empirical relationships for the penetration length (10). Weimer, et al., using a variable density single fluid model for the two phase flow, with the turbulent mixing process treated by an entrainment law found good correlation with results of their experiments and those of earlier investigators over a wide range of operating conditions and injector geometries.

Avery (12) considered the case of a gaseous oxidizer jet discharging through an injector subjerged in a bath containing a liquid metal. The two phase turbulent combustion process was analyzed in a manner similar to conventional diffusion flames. A variable density single fluid model was used to represent the two phase mixture in conjunction with an entrainment assumption appropriate for systems with large density differences between the jet and ambient fluid. The theory provided a general relationship for estimating combustion and condensation lengths for turbulent, unconfined, forced jets based on injector and ambient properties. Results indicate that mixing characteristics of gas-liquid jets when corrected for density variations are similar to single phase jets.

Thomson (1) studied the heat transfer for a jet induced mixing process in a cylindrical chamber. A heated fluid was injected centrally from one end of the chamber into a liquid bath. Both ends of the chamber were insulated so only heat transfer through the side wall was considered. Data was obtained for water and ethylene glycol,

varying the injector diameter, fluid temperature, jet momentum and chamber dimensions. An analysis assuming total jet momentum dissipation into shear stress along the chamber wall was developed using the Reynold analogy to determine the characteristic parameters of the system. Good agreement between the analysis and data set was obtained. From the analysis, the data was correlated in terms of a Stanton number, Reynolds number, Prandtl number and chamber length to diameter ratio.

Gosman, et al. (13) present numerical solutions for seven different two dimensional turbulent elliptic flows. The solution procedure employed is that embodied in the TEACH computer program (14). The calculated properties of the seven flows were compared with experimental results which validated the numerical procedure and the two equation turbulence model described by Launder et al. (15). Of particular interest here is their investigation of flow downstream of an axisymmetric, sudden enlargement in channel flow. The flow structure is only slightly different from that in the SIR. They observe strong recirculation and their results compare well with the measurements of Back and Roschke (16).

There has also been a substantial amount of work on flow visualization in mixing vessels. Reynold (17) used a dye to visualize a jet directed into a water bath. Jet breakdown was observed as a function of Reynolds number. Reynold observed five categories of flows which he classified as (going from lower Reynold numbers to higher ones), shearing puffs, symmetric condensation, sinuous undulations, pedal

breakdown, and confused breakdown (at Reynold numbers higher than 300).

McNaughton and Sinclair (18) studied liquid-into-liquid jets in short cylindrical vessels using aqueous blue tracer solution in conjunction with transparent cylinder walls. Four main types of jets were observed: dissipated laminar jets (Reynold numbers less than 300), fully laminar jets (Reynold numbers between 300 and 1000), semi-turbulent (Reynold numbers between 1000 and 3000) and fully turbulent (Reynold number greater than 3000). The laminar length of sub-turbulent jets was investigated and correlated with the Reynolds number and geometric parameters. Crow and Champagne (19) also used dyes to study the evolution of jet instability with advancing Reynolds number. They also employed schlieren and light scattering visualization techniques to study the jet structure.

Back and Roschke (16) investigated the flow of water through an abrupt circular channel expansion. The shear layer between the central jet and reverse flow region along the wall downstream behaved differently in the observed regimes. Dye injection into the shear layer provided a means of observing the jet reattachment lengths in the various regimes from laminar to fully turbulent. The reattachment lengths were found to increase from laminar flow to reach a maximum and then decrease for highly turbulent flows.

White, et al. (20) used a particle visualization technique to study the recirculating flow of a submerged jet discharging into a dead ended vessel. They used this to study the tangential vorticity, and the visualization study was not extensive. A similar study was carried out by Ekhcian and Hoult (24) to study the intake process in

an internal combustion engine.

Numerous other authors have done work similar to what has been discussed in this section. However no paper directs itself at obtaining an understanding of the overall flow structure in jet stirred baths.

1.4 Scope and Objective of this Study

From this discussion, it is evident that a better understanding of the flow structure in the SIR is needed. The purpose of this investigation was to visualize the flow structure in the SIR in order to obtain such qualitative information.

In order to simulate the SIR, water was injected axially into a cylinder which provided for a variable outflow at both ends at a low momentum flux. The flow was seeded with fine alumina particles, a high intensity light source with a condensing lens focused a thin plane of light onto a cylinder axis. A camera located perpendicularly above this illuminated plane recorded the flow pattern at various inlet momentums and outflows (at the two ends). Dye visualization techniques were used both in the jet and in the shear layer, but with limited success.

An analysis was carried out using a modified form of the TEACH computer program (13,14). Velocity, pressure, turbulent kinetic energy and dissipation profiles were obtained for the SIR geometry as a function of Reynold number. A comparison is made between experimental and analytic trends.

CHAPTER II

THEORY AND ANALYSIS

2.1 Analog Technique

A water model was employed to simulate the flow field in a SIR, so as to facilitate flow visualization. In order to conduct such an investigation with a water model, it is necessary to satisfy the similarity conditions (21).

Similarity can be classified as follows:

1. Geometric similarity
2. Kinematic similarity
3. Dynamic similarity
4. Thermal similarity

Geometric similarity requires a single scale ratio between critical dimensions of the prototype and model. In the case of the SIR-model this scale ratio is taken as unity, hence satisfying geometric similarity.

Kinematic similarity requires that the slopes of the streamlines are the same in the model and the prototype, implying that the corresponding flows are alike. The assumption that the fluid in both cases are incompressible (assuming the compressibility effects in the gaseous oxidizer are negligible) leads to the conclusion that the continuity equation and hence the streamlines are identical for the prototype and model (22).

Dynamic similarity requires that the forces acting on the fluid elements have the same ratio to each other at any instant. In the SIR bath both inertia and viscous forces are of importance, and it would seem logical to conclude that the Reynolds numbers should be equal for the model and prototype. This would involve the problem of determining the Reynolds number for a two-phase system. This problem is avoided by considering that the inertia forces in the jet are of greater significance (high Reynolds numbers) than the viscous forces in the jet. The injector momentum flux for the model was taken as the same momentum flux that is present in the SIR. This established an injector velocity range for the model corresponding to the operating range of the SIR.

Thermal similarity is of no consequence in this study. It was concluded that with an injector velocity range selected as in this similarity discussion, the velocity field in the model would relate well to that existing in the SIR. Hence, it seems to be worthwhile to conduct an analog experiment with water injected into water.

2.2 Analysis and Computer Code

A special case of the SIR, where the inflow and outflow are on the same end of a dead ended cylinder was considered in this analysis. Figure 1 depicts the geometry. The analysis was carried out using a modified form of TEACH.

TEACH-T is a form of the more general program TEACH and is used specifically for computation of flows in ducts with sudden enlargements.

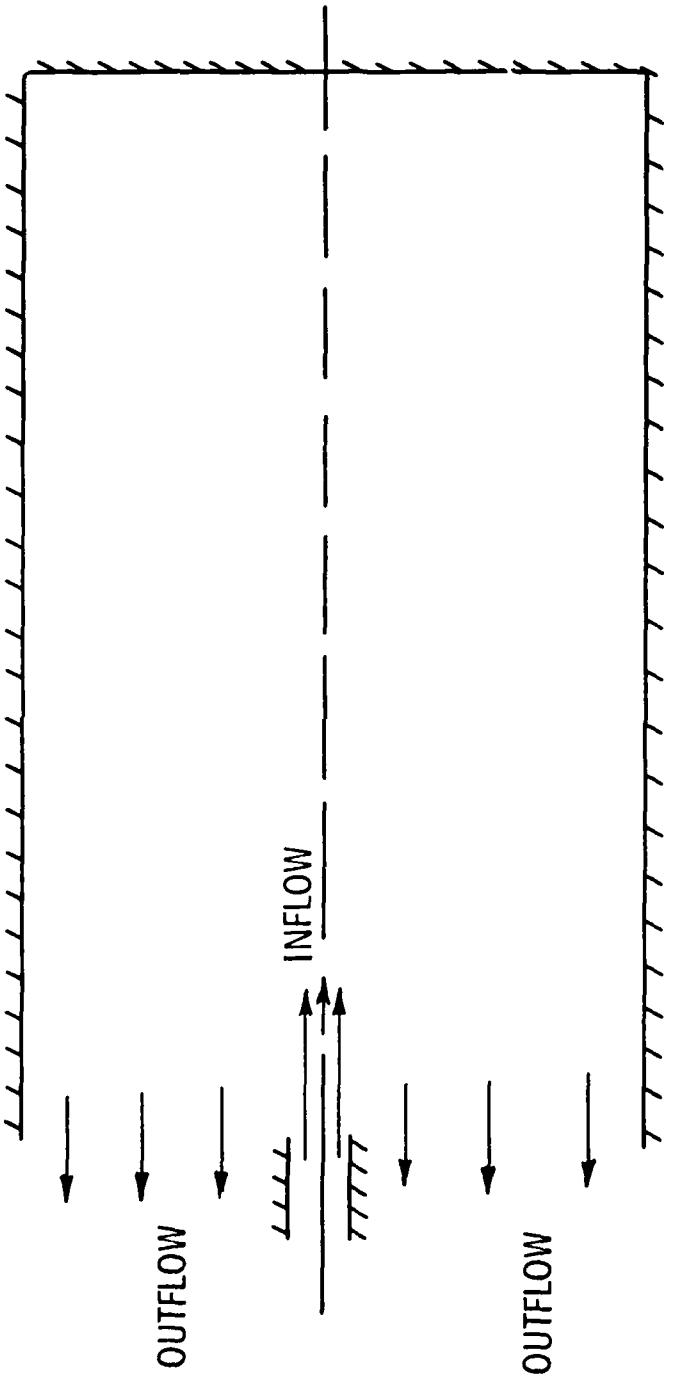

Fig. 1 Dead Ended Model Considered in the Analysis

Modifications were made to TEACH-T to account for the geometry of the SIR. Refer to Gosman, et al. (13) for a more detailed description of TEACH-T.

In TEACH-T the geometry is as that of Figure 2, which shows the region of flow bounded by the duct walls, the axis of plane of symmetry, inlet and outlet boundaries. The inlet boundary is located in the plane of the step, where the conditions of the incoming fluid are presumed to be known; while the outlet boundary is positioned sufficiently enough downstream that the assumption of fully developed flow is fairly accurate.

The inflow is presumed to be steady and turbulent, with a mean velocity $\bar{U}_{in}$. The diameters of the large and small ducts are designated by D and d respectively.

The predictions of the problem require the solution of the equations of motion for axial velocity U, radial velocity V, pressure P, together with the two equation model for turbulent closure involving turbulent kinetic energy, k, and dissipation, ε.

The numerical technique and constants were retained in their entirety, slight changes were made in the grid size. The only major modifications made to deal with the model of Figure 1 were changes in the boundary conditions. The following guidelines were used when making changes in the boundary conditions:

1. Profiles for U, V, P, k and ε are supplied at the inlet plane.
2. At the boundary walls, the calculation of the velocity component parallel to the wall, turbulent kinetic energy, and dissipation are made using a logarithmic law of the wall,

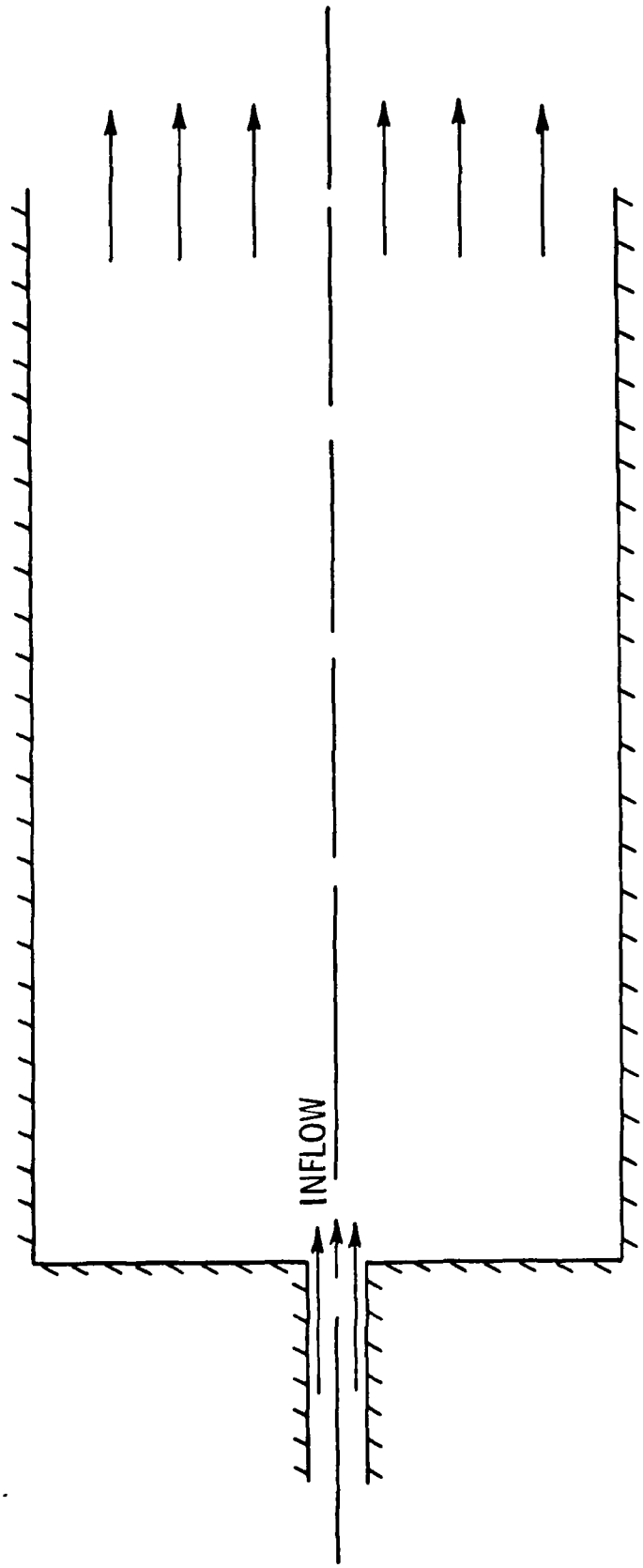

Fig. 2 Flow in Duct with Sudden Enlargement as Considered in TEACH-T

as in the original program.

3. At the axis of symmetry, the condition of vanishing normal flux is applied to all variables.
4. At the outlet plane, the normal velocities are deduced from the overall mass continuity requirements and specification of a fully developed velocity profile.

Basic changes to be made in the boundary conditions were two-fold:

1. Introduction of an end wall at the desired location using the corresponding boundary conditions.
2. Removal of the boundary condition at the existing side wall and replacement with an outflow condition.

This called for changes in two parts of the program TEACH-T. Modifications were made in the main program to define the initial variable distributions to change geometry (example, ratio of d to D) and to define new variables and changes in format statements. Changes were also required in SUBROUTINE PROMOD, responsible for the modification of the finite difference equation terms and coefficients at the boundaries. Changes in the individual sections of this subroutine are described as follows:

1. ENTRY MODU: responsible for modifications for calculation of the axial velocity. The conditions at the top wall and axis of symmetry remain the same. The outlet boundary is replaced with an end wall; as shown in Appendix A, the value

of the coefficient of the finite difference equation is calculated and introduced in this section. The existing side wall conditions are removed and replaced by an outflow condition. Two outflow conditions were tried. In one, it was assumed that the exit velocity profile was fully developed; in the other, an exit velocity profile was assumed at the outset.

2. ENTRY MODV: responsible for modifications for calculation of the radial velocity. Side wall conditions were introduced in accordance with the law of the wall as shown in Appendix A.
3. ENTRY MODTE: responsible for modification for calculation of turbulent kinetic energy. Side wall conditions were introduced in accordance with the law of the wall as in ENTRY MODV.
4. ENTRY MODED: responsible for modification for calculation of dissipation rate. Side wall conditions were introduced in accordance with the law of the wall as in ENTRY MODV.

All other parameters remained unchanged. A list of the modified statements is included in Appendix B.

CHAPTER III

EXPERIMENTAL PROCEDURE

3.1 Experimental Method

Qualitative information on the flow structure in the model was obtained using a particle visualization technique similar to the one presented by Ekchian and Hoult (24). Their method utilized neutral density particles to study the flow structure in the water analog of an internal combustion engine. Allen and Yerman (25) found that neutral density particles do not alter the flow field; quantitative velocity predictions made from their technique were within five percent of pitot tube data. In this study alumina particles were used; which for small enough particle sizes can be expected to follow the flow as well as neutral density particles (26,27).

A two dimensional flow field was assumed, and a plane containing the axis of the model was assumed to be representative of the flow structure in the entire flow field. A plane so described was illuminated at a high intensity. The width of the illuminated zone was made small in comparison with other dimensions and it was assumed to be a plane. The particles (assumed to move along streamlines (26)) were photographically recorded as they passed through the illuminated plane, yielding a picture of the instantaneous flow structure.

3.2 Experimental Components

Figure 3 is a schematic diagram of the water loop. The major

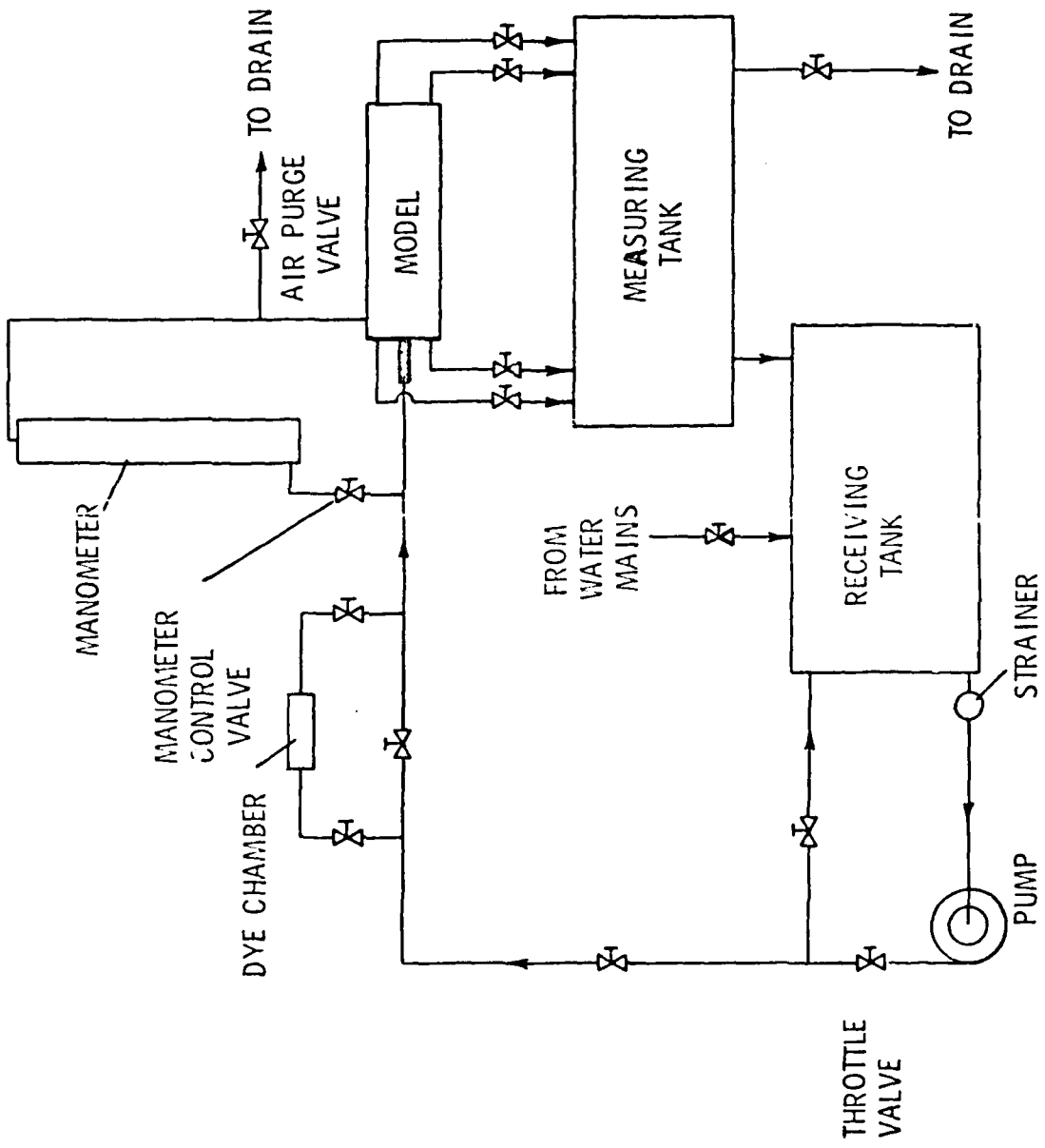

Fig. 5 Schematic of the Water Loop

component of the apparatus was the horizontal cylindrical test chamber (model). The fluid jet was injected centrally from one end of the chamber, and fluid was continuously discharged through small holes on both ends. The other components included a measuring tank, receiving tank, dye bypass, centrifugal pump, valves and a differential manometer.

The working fluid, water, was pumped through a strainer and an injector into the model. A mercury filled differential manometer used across the injector nozzle was calibrated to determine the injector velocity. When the line to the dye chamber was opened, water mixed with green dye (Merriam #D-2930) and was injected into the clear bath gave a picture of the spreading jet.

Outflow from the model could be controlled using the valves on either end of the model. Volumetric flow rate was measured using a stop watch (least count of a hundredth of a second) and the measuring tank. When dye studies were performed, the colored water was drained out of the measuring tank, the water loop was open. For the particle visualization studies, i.e. water in the receiving tank was seeded with alumina particles and the tank was kept stirred; water from the measuring tank was not drained, but let into the receiving tank instead.

Air in the model was removed by opening the air purge valve on the manometer line. When this valve was opened, the manometer was isolated from the rest of the system by shutting the manometer control valve.

Figure 4 is a picture of the water loop as set up. A more detailed description of the individual components follows.

3.2.1 Model of SIR

The model was used in two basic configurations; the first one so as to enable dye injection with a syringe at various wall locations downstream of the injector plane, the second one for particle visualization.

The model consisted of a visualization cylinder cut out of a plexiglass tube (Cadco Acrylic). The tube had an outer diameter of 4.25 inches and an internal diameter of 3.5 inches. A 6 inch long cylindrical tube was used for the dye studies and 13.25 inch long one for particle visualization, giving length to diameter ratios of 1.71 and 3.50 respectively.

Figure 5 shows a visualization cylinder as used for the dye visualization studies. A pressure tap was located 0.5 inches from the end on the top of the cylinder wall, and numerous other taps, fitted for syringe injection were located along the cylinder wall. The injection fittings were made by adapting standard fittings as shown in Figure 6. The glands ensured that there was no leakage out of the model, the needle guide ensured that the needle (which was 6 inches long) did not buckle when pushed through the gland. Both ends of the visualization cylinder were tapped axially for twelve equally spaced 10-32 screws. Only the pressure tap existed on the cylinder used for the particle visualization studies.

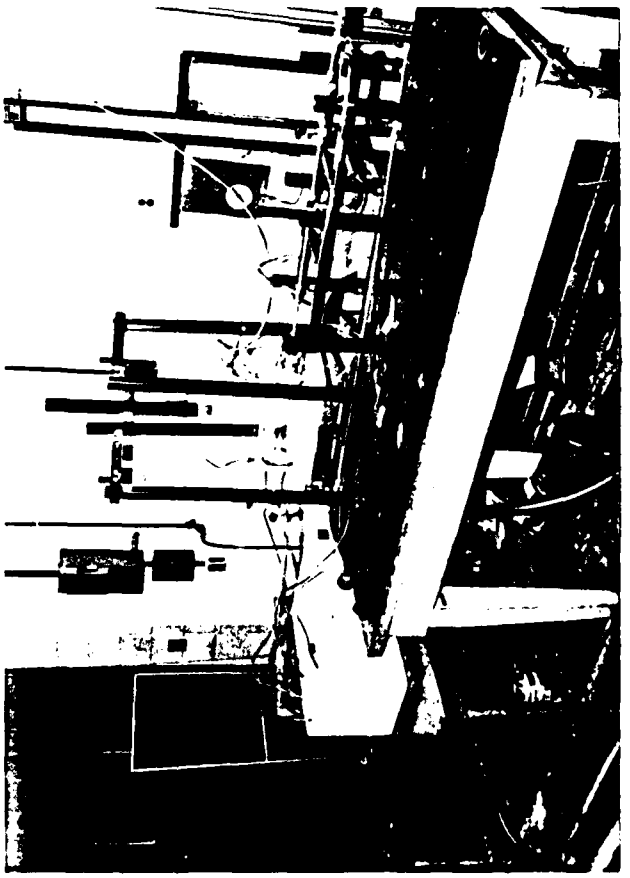

Fig. 1 Picture of the Water Loop as Set up in the Lab.

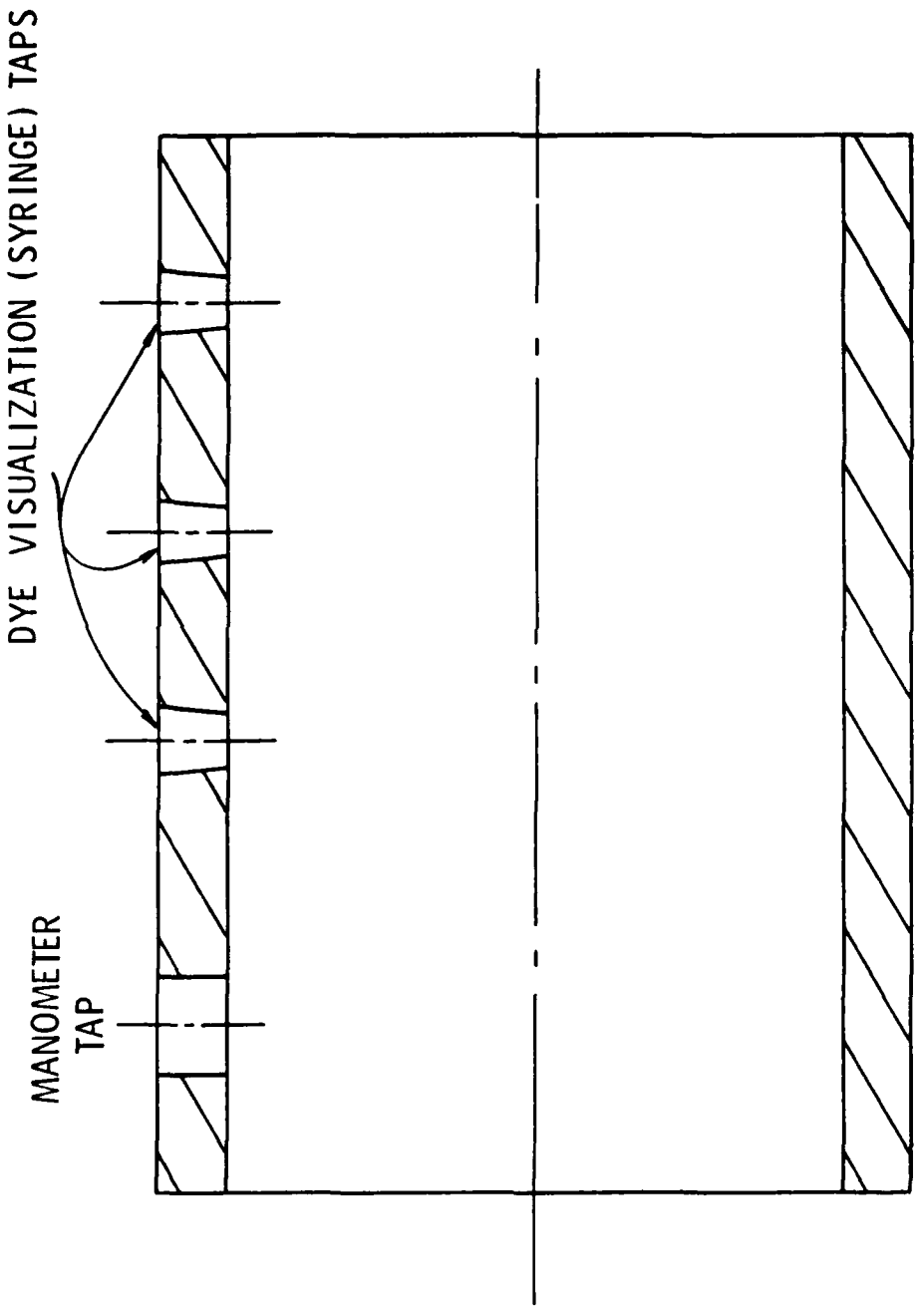

Fig. 5 Visualization Cylinder for Dye Injection

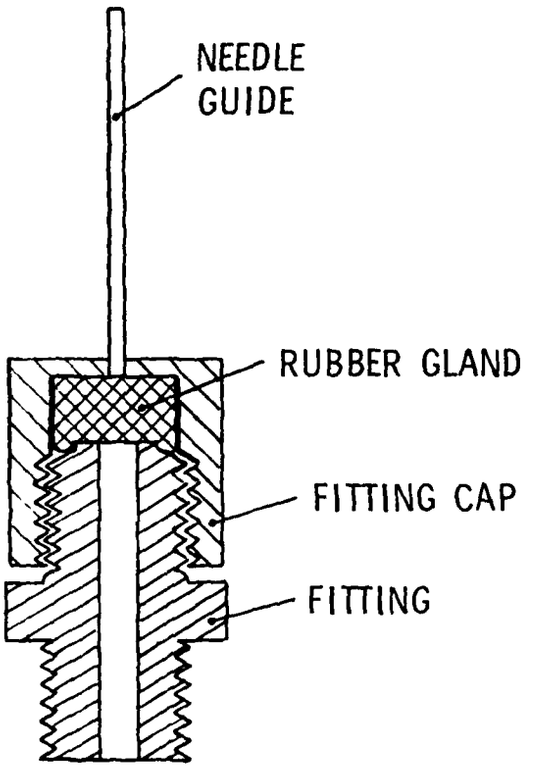

Fig. 6 Cross Section of Dye Injection Fitting

The visualization cylinder was used in conjunction with end caps, perforated plates, rubber gaskets, visualization box end plates and a nozzle, assembled as shown in Figure 7 (picture). Figure 8 shows the schematic of the same.

The visualization box is used in the case of particle visualization studies, when filled with water it removes most of the distortion in photographs caused by the curvature of the cylinder.

Figure 9 shows a perforated end plate, cut 0.25 inches thick from a 4.5 inch diameter plexiglass rod (Cadco Acrylic). The perforations are 0.125 inch in diameter, set out in a 0.5 inch x 0.5 inch matrix as shown. Aluminum rivets, either blank or with through holes fit into these perforations, allowing for control of the outward mass flux distribution. The diameters of the holes in the rivets were 0.016 inch, 0.025 inch, 0.031 inch and 0.033 inch.

The end caps cut from a 4.5 inch diameter plexiglass rod were machined to shape. They provided outlets for outflow to the measuring tank.

The nozzle was machined down from a 1 inch brass bar stock; it had a 0.5 inch outer diameter and a 0.0995 inch hole diameter. It was 5 inches long and was held in place using a teflon compression fitting screwed into the end cap.

The entire assembly was held together by two sets of 10-32 screws, one set on each end.

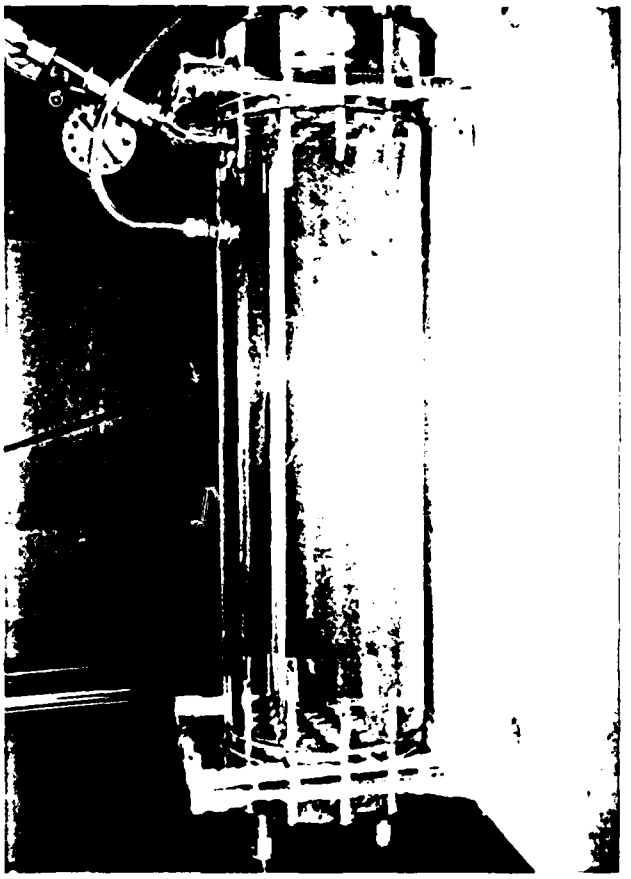

Fig. 7 Picture of Model

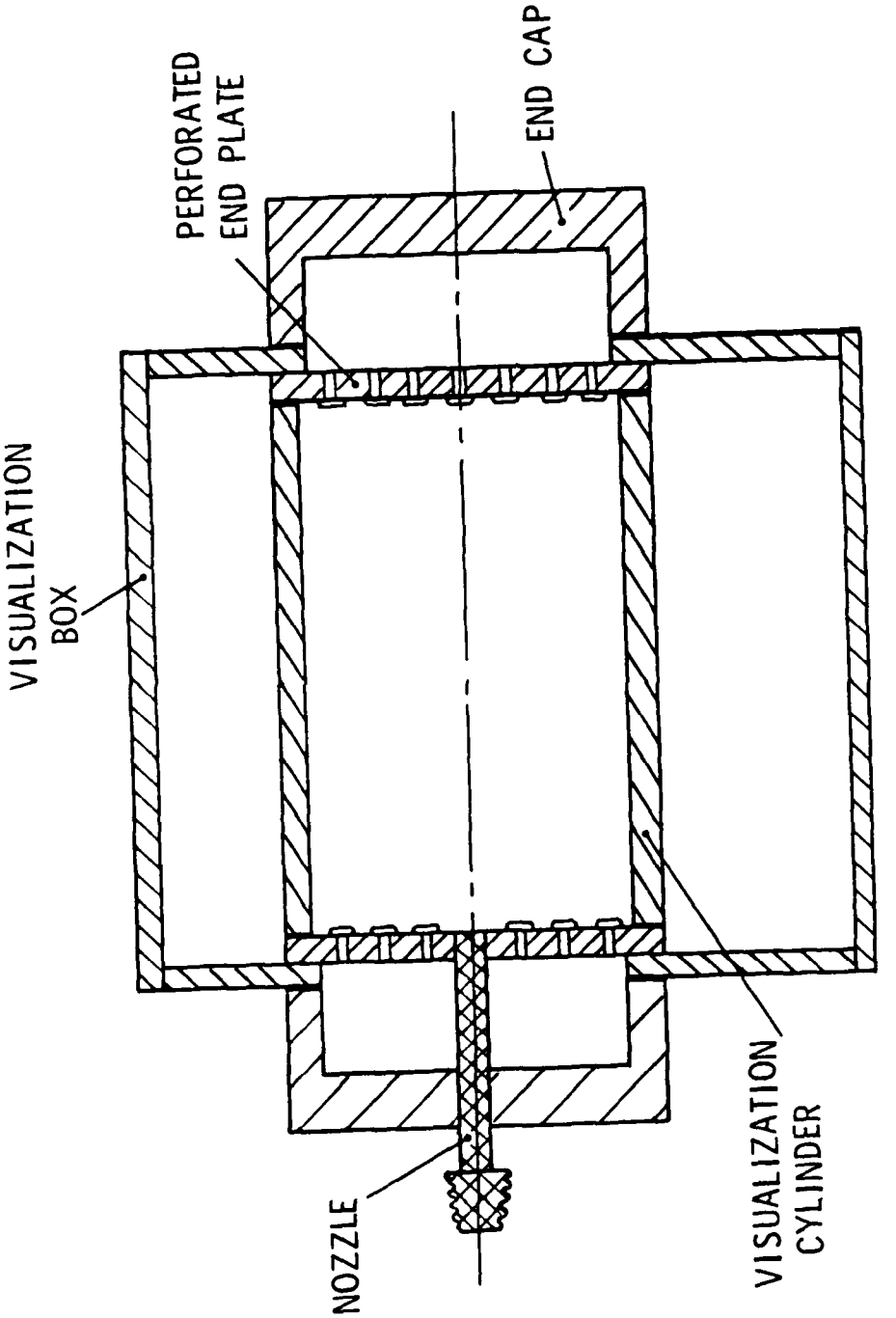

Fig. 8 Schematic of Model Assembly

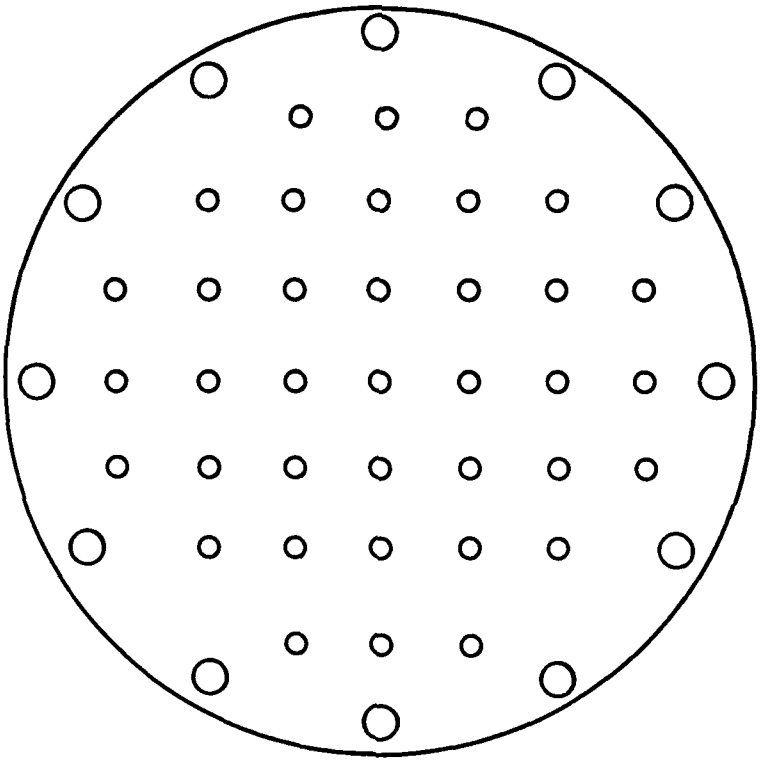

Fig. 9 Perforated End Plate (front view)

3.2.2 Dye Bypass

Figure 3 shows a dye bypass loop. It was used when dye injection through the nozzle was desired. It was possible to divert all the flow or a part of the flow through this bypass where it picked up the green dye on its way to the injector. The bypass had three control valves as shown in Figure 3 and a dye container which had to be recharged after each run.

3.2.3 Differential Manometer

A Meriam Instruments 60 inch mercury differential manometer was calibrated to give the injector velocity as a function of the pressure drop across the nozzle measured in inches of mercury.

3.2.4 Measuring and Receiving Tanks

A plastic measuring tank with dimensions 12 inches x 12 inches x 12 inches was used with a stop watch to measure the volumetric flow rate in the water loop. It was possible to measure separately the water flow rate coming out of each end of the model. This tank emptied into the receiving tank for the particle visualization runs, for dye studies this tank was cut off from the receiving tank and all the water was drained out. The mean water temperature was found to be 70°F.

The receiving tank was also made of plastic, slightly larger in size, 20 inches x 24 inches x 24 inches and normally held 110 litres of water. Alumina particles were seeded into the water loop through this tank which was kept well stirred. A wire mesh at the tank outlet acted as a strainer, but let the small alumina particles through.

3.2.5 Forced Circulation Pump

The water flow through the loop was driven by a pump located downstream of the receiving tank. The pump manufactured by the Allis Chalmers Corporation was a centrifugal pump with a maximum rpm of 3450. It was driven by a 0.75 HP close coupled electric motor. It could provide a maximum flow rate of 1.76 litres per second. The flow rate through the system was controlled by means of a throttling valve on the pump discharge.

3.2.6 Visualization Box

A rectangular plexiglass box of dimensions 5.5 inches x 4.75 inches x 14 inches was used to enclose the visualization cylinder when conducting particle visualization studies. The box was constructed from 0.25 inch thick plexiglass plates glued together and made watertight by using silicon sealant. The end plates of this box fitted into the model assembly between the perforated plate and the end plate as shown in Figure 8. This box had two ports on the top, one for water feed and the other for air escape. It had a drainage port on the bottom. When filled with water, it removed most of the optical distortion caused by the curvature of the cylinder and enabled good photography. This box was not used when doing dye visualization studies.

3.3 Lighting Equipment

The light source consisted of a 115V, 10 amp General Electric mercury-arc-capillary lamp, lamp housing, transformer and tripod. The lamp emitted high intensity ultraviolet radiation. The lamp and housing were both air cooled, using air throttled from the machine

shop air supply at 55 psi. The cooling was monitored by a General Electric mercury lamp control unit which operated on 115V, 400 Hz power supply, obtained using a brushless inductor/alternator made by the Leach Co.

The lamp housing also contained a system of parallel slits and plano-convex condensing lenses, which enlarged, collimated and defined a thin light beam.

The light source and lenses in a single housing were mounted on a tripod as shown in the picture of Figure 10. This allowed for raising or lowering and swivel motion of the light housing.

The slits transformed the light into a plane containing the axis of the model. The light was shielded so as to prevent light leaving from anywhere else except the slit.

3.4 Photographic Equipment

A 35 mm Canon AE-1 camera was used to photograph the illuminated particles through the transparent visualization box. The camera was used in conjunction with a 12 mm Vivitar extension tube so as to allow undistorted close-up photography. The camera was mounted 10.1 inches vertically above the model axis and the focus was set at infinity to give a sharp and clear picture. Provisions were made for lateral movement of the camera, so the entire flow field could be photographed using exposures at the different locations along the axis of the model. Figure 11 shows the camera position relative to the light source and visualization box.

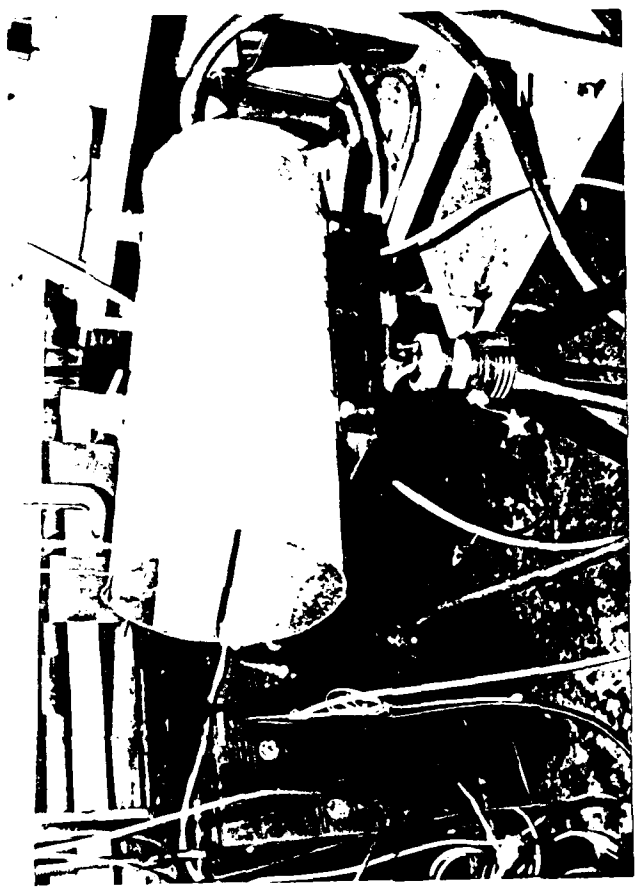

Fig. 10 Picture of the Lamp Housing on the Tripod and the Lamp Control Unit

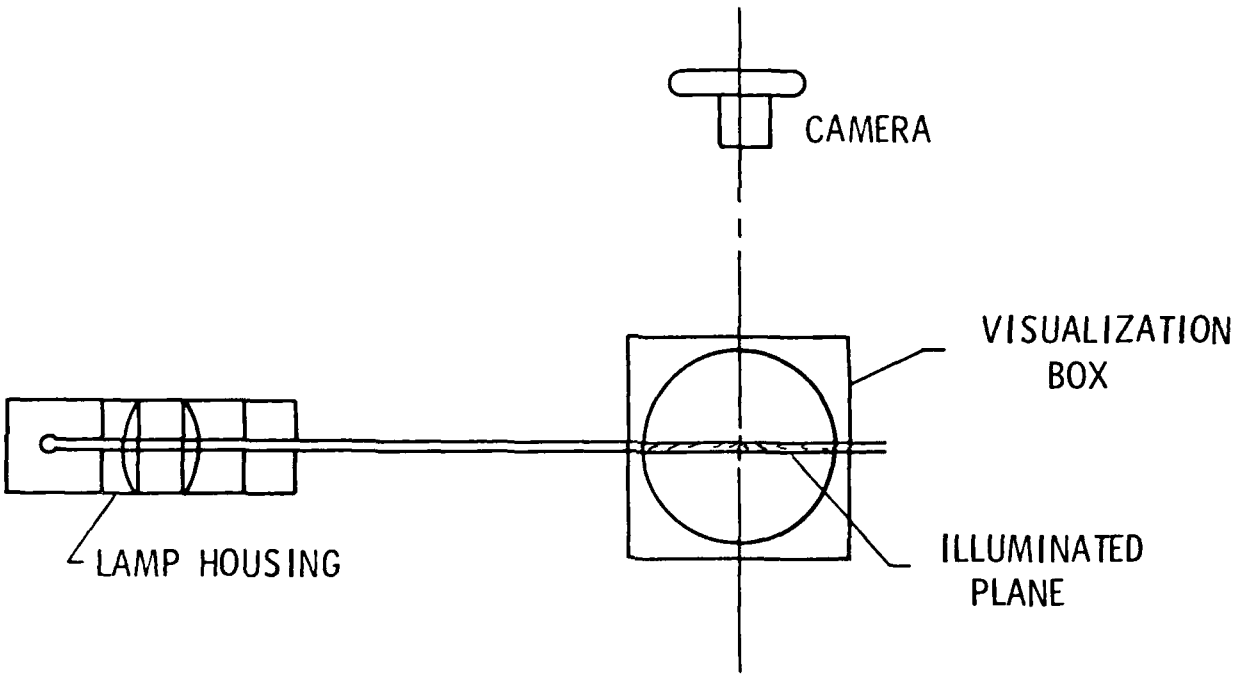

Fig. 11 Cross Section Showing the Relative Positioning of Components for Particle Visualization.

3.5 Visualization Particles

To make the flow in the model visible, small alumina particles were used as the seed particles to be tracked. The alumina powder used was supplied by Atomized Metal Powders, Inc. The particles, though not neutral density, were very small and [illegible] in a diameter range of 30 to 40 microns.

Alumina particles have high reflectivity and have been used by numerous investigators, such as [illegible]. It is essential for a particle to follow the flow well, that is have small values for sinking velocity. The sinking velocity is directly proportional to the square of the particle diameter, and to the difference between the particle and fluid density; it is inversely proportional to the fluid viscosity [20]. Though the density match between alumina and water is not too good, it is compensated for by using very small particle sizes. The residence time of a fluid element in the model is so small that sinking is almost non-existent. Thus, such particles are expected to map the flow well.

The traces of the particles as seen on the photographs were projections of their paths into a plane containing the axis of the model. The particles were seeded into the waterloop through the receiving tank which was kept stirred.

3.6 Photography

Optimum photography was obtained using a Kodak Tri X film (TX-135-20) which was black and white film exposed and developed at 400 ASA. The

optimum camera setting was obtained at a shutter speed of 1/15 seconds and an aperture f8.0 when the light slit was 8 to 10 mm wide.

The negatives were used to project an image on a screen using a film strip projector.

CHAPTER IV

PRESENTATION AND INTERPRETATION OF RESULTS

4.1 Dye Visualization Experiments

Two techniques were used for dye visualization studies in the model. In one case, a dye-water mixture was injected into a clear bath in the model, through the nozzle. In the second case, a syringe was used to inject pure dye into a clear bath in the model, through glands fitted to the model wall.

4.1.1 Nozzle Dye Injection

Test runs were made using inlet velocities ranging from 2 m/s to 18 m/s. These velocities corresponded to those in the SIR applying the similarity conditions of Chapter II. The corresponding inlet Reynolds number range was from 4170 to 46530. According to McNaughton and Sinclair (18), for inlet Reynold numbers greater than 3000 for liquid-liquid jets in short cylindrical vessels, fully turbulent jets are observed. Indeed, these dye visualization studies did reveal a turbulent jet, comprised of a forward moving conical jet region and a slower moving backflow region which surrounded the jet. No laminar length was observed, and the jet mushroomed at the point of injection.

The dye used was neutral density and was assumed to follow the streamlines. The technique however could not provide more detailed information in this case due to the diffusivity associated with turbulent flows. High flow velocities caused the entire bath to cloud in a fraction of a second, further limiting the effectiveness of the technique. These experiments established that the jet was turbulent

and that recirculation was predominant.

4.1.2 Syringe Dye Injection

This technique was intended to help in gaining insight into the reattachment lengths of the turbulent jet. It was also hoped that this method would provide a means of isolating particular regions in the flow that were of interest. A similar technique was used by Back and Roschke (16), in which dye was bled into the shear layer between the jet and reverse flow region, through holes in a circular channel wall unstream of a sudden expansion. Their studies were limited to a Reynold number range from 20 to 4200.

Dye was injected into the bath at various locations downstream of the nozzle. The syringe was inserted to different depths and the dye released. By releasing dye at a given axial location, but varying radial locations, the shear layer was located at the point above which the dye moved in the reverse direction and below which the dye moved with the jet flow. When dye was injected into the shear layer, it was expected to follow it until it reattached at the cylinder wall at some downstream location. Unfortunately, due to the high turbulence intensity and fluctuating flow pattern such observation was not clear. At lower Reynolds numbers (about 5200 to 7000) it was possible to infer that the flow did not reattach to the cylinder walls; when it approached the end of the cylinder the dye seemed to turn and a part of it would flow back along the cylinder wall. It must be pointed out that due to the clouding of the dye at the end of the cylinder and due to the fluctuating location of the shear layer, such inferences are not

very obvious and could be questioned. These inferences however seem to be in agreement with Back and Roschke's predictions that reattachment occurs about 9 to 10 step heights downstream of injection for turbulent jets; in this case the cylinder was only 3.5 step heights long.

This technique established the fluctuating nature of the flow and that numerous eddies existed in the reverse flow regions. These eddies were isolated since they would contain dye injected into them for a small length of time until fluctuations caused the eddy to disappear. This time period was not long enough for detailed observation. The need was felt for obtaining an overall picture of the flow structure and to observe how this overall structure fluctuated.

4.2 Particle Visualization Experiments

Illuminated alumina particles were used to visualize the flow field in the model with a length to diameter ratio of 3.5. The experiment was run in the jet Reynolds number range similar to that in the dye experiments. Outflow at both ends of the model was varied.

Figure 12 shows the typical flow pattern observed. The flow consisted of a spreading jet, a strong recirculating back flow near the wall, and numerous eddies which appeared and disappeared in less than 1/10 of a second. These eddies caused the jet flow to bend around them, their appearing and disappearing causing a side to side whipping motion of the jet. It seemed that the jet whipped from one wall to another in an almost regular manner. This whipping was stronger for higher Reynolds numbers but was confined to a region near the extreme

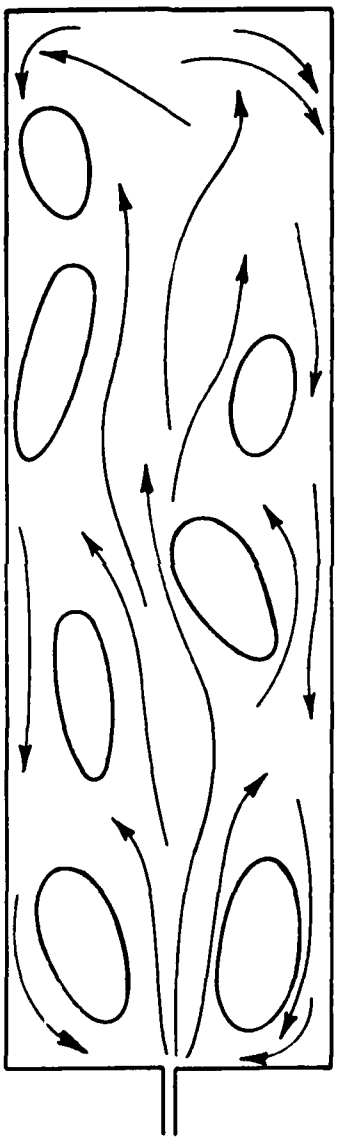

Fig. 12 Typically Observed Flow Pattern

end (away from the injector) of the cylinder. For small Reynolds numbers, the whipping was weaker but was prevalent in the entire flow field; in this case the jet would whip in a serpentine manner. These observations are not obvious from Figures 13, 14 and 15 as these figures represent instantaneous flow pictures.

Figures 13, 14 and 15 provide the contrast between varying outflow at either end. All three pictures represent an inlet Reynolds number of 7057. The three frames in each picture represent three segments of the model each photographed separately and at different instants of time.

Figure 13 shows the case where all the outflow is on the extreme end of the model. The jet entrainment near the injector end can be seen. Recirculation is not very strong compared to the case of Figure 15, in which outflow is all on the injector end. Alumina particles tend to accumulate at the extreme end where they are discharged. One can observe a lot of eddy structure in the central segment, surrounding the high velocity jet core which is wrinkled and broken.

In Figure 15, not many particles are visible in the backflow region along the walls due to the high velocities existing in this case which makes it difficult to record the particle motion at the given level of illumination. In this case a stagnation region is observed at the extreme end and particles can be seen to turn away from the direction of jet flow into the reverse flow region. In this case the number of eddies existing are not as many as in Figure 13. Jet entrainment is evident.

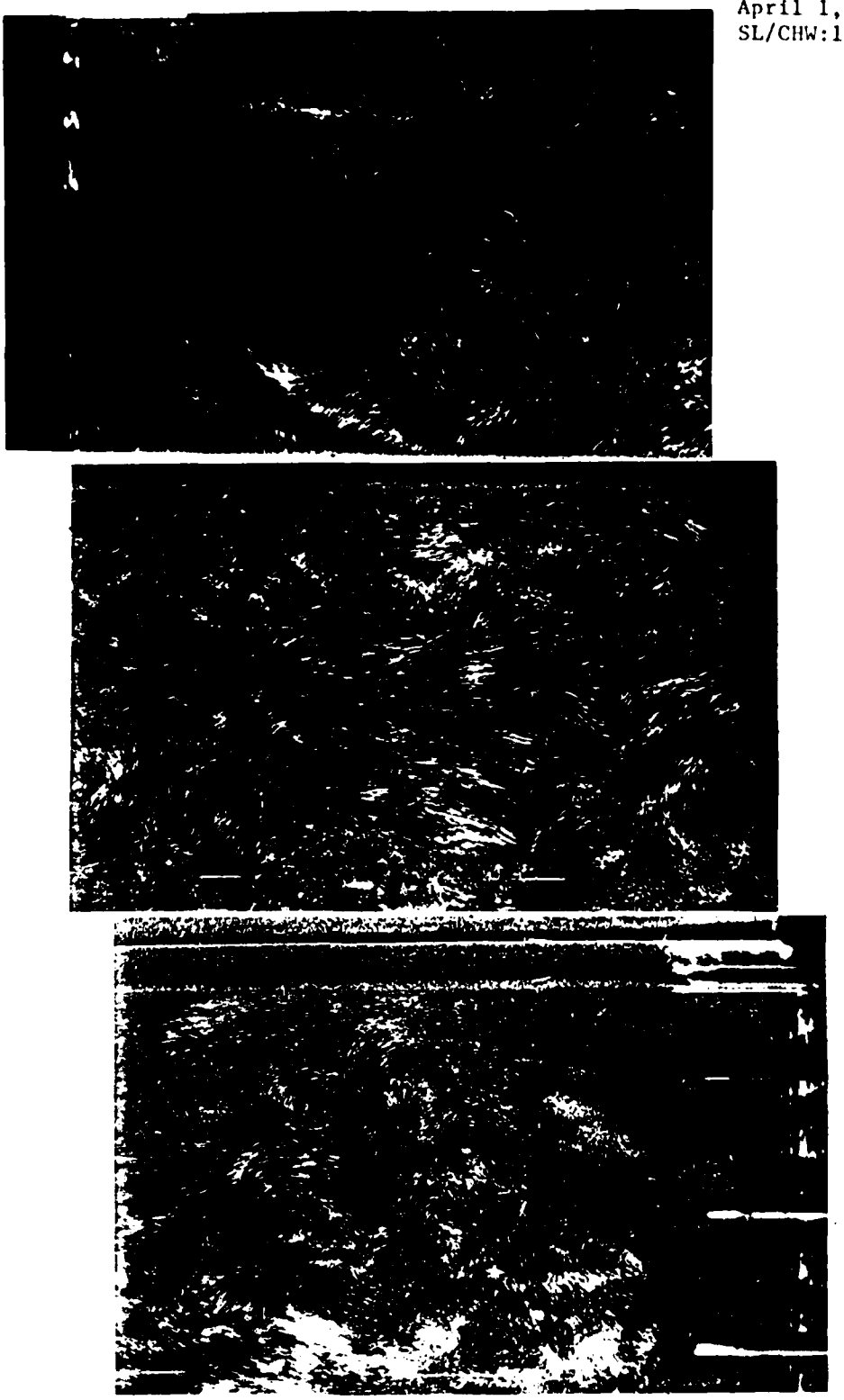

Fig. 15 Picture of Flow Field at Reynolds Number 7057

(outflow on extreme end)

April 1, 1980
SL/CHW:lcl

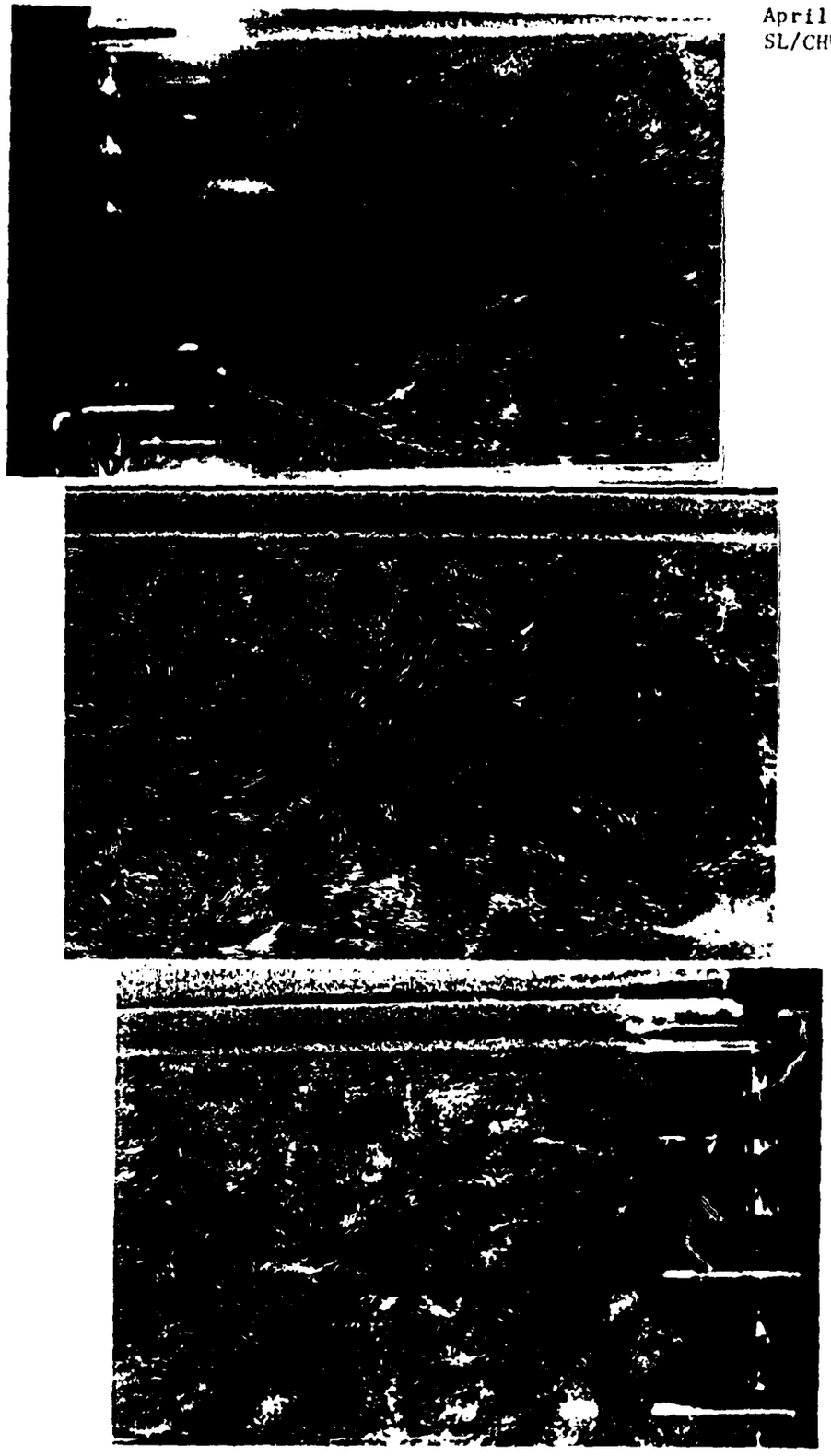

Fig. 11 Picture of Flow Field at Reynolds Number 7057

(outflow equally divided between both ends)

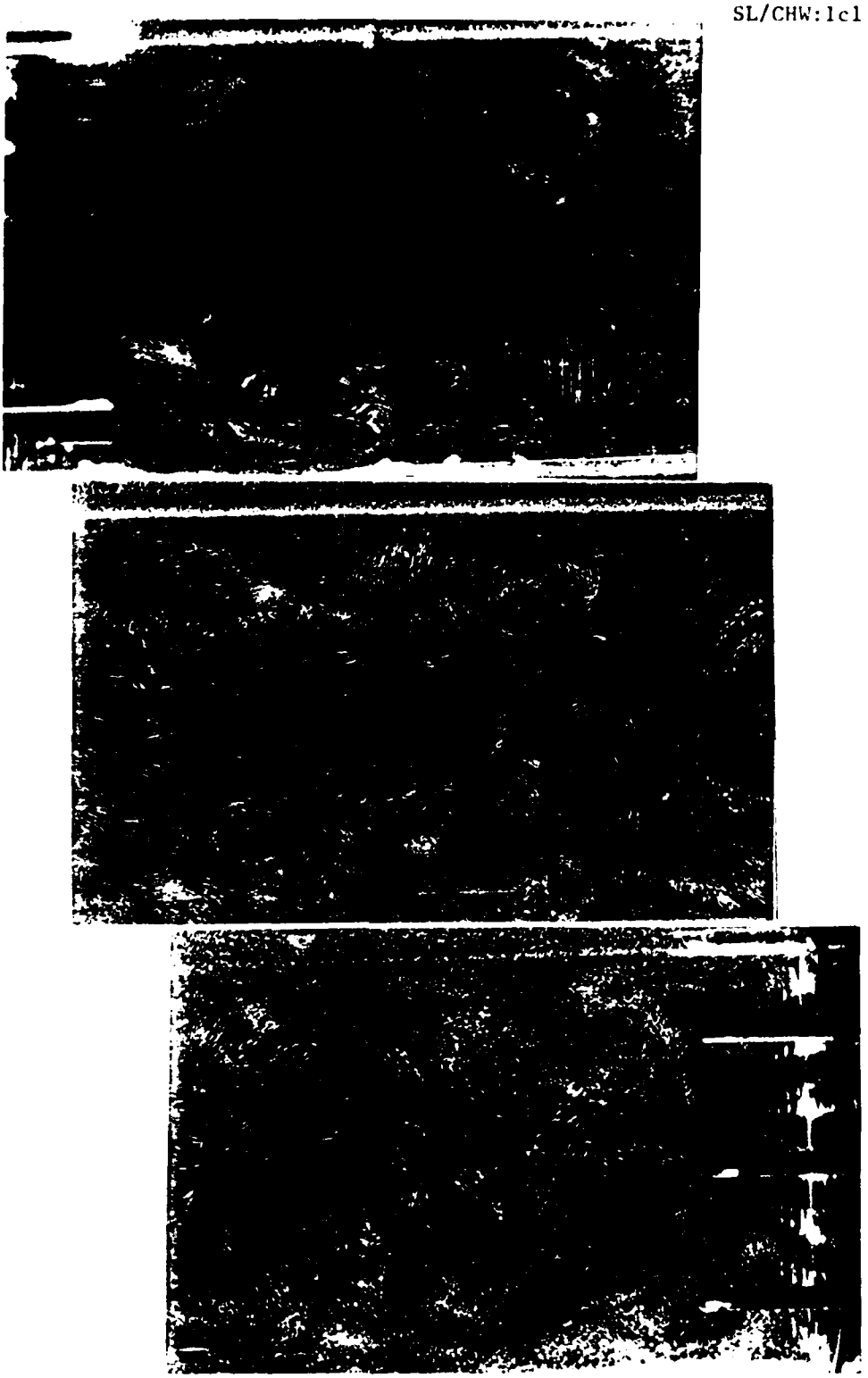

Fig. 15 Picture of Flow Field at Reynolds Number 7057

(outflow on injector end)

Figure 14 shows the case where the outflow is equally divided between the two ends of the model. It does seem that this case is between those of Figures 13 and 15. Particle accumulation is absent at the extreme end and the reverse flow velocity near the wall becomes large only for the near injector region. Eddies and wrinkled jet structure are predominant in the central segment.

It is concluded that the outflow configuration is of major consequence in determining the flow structure in the model.

The effect of higher Reynolds numbers was studied. Figure 16 shows the picture of the flow structure for a Reynolds number of 32315, it is the case with all the outflow on the injector end and is compared with the similar case (Figure 15) for a Reynolds number of 7057. The higher Reynolds number case shows a highly turbulent jet with a high velocity backflow. There is high jet entrainment in the near nozzle region and a resulting high spreading rate of the jet. A lot of small eddy structure is visible in the extreme end region. This is in contrast with the lower Reynolds number cases where eddy structure was predominant throughout the length of the model. Figure 17 shows the same outflow configuration for a jet Reynolds number of 18095. The overall structure remains the same, small eddy structure is ovserved even in the central segment.

4.3 Results from the Modified TEACH Computer Code

TEACH was run for the model using a water analog with outflow only on the injector end, the extreme end was a region of stagnation.

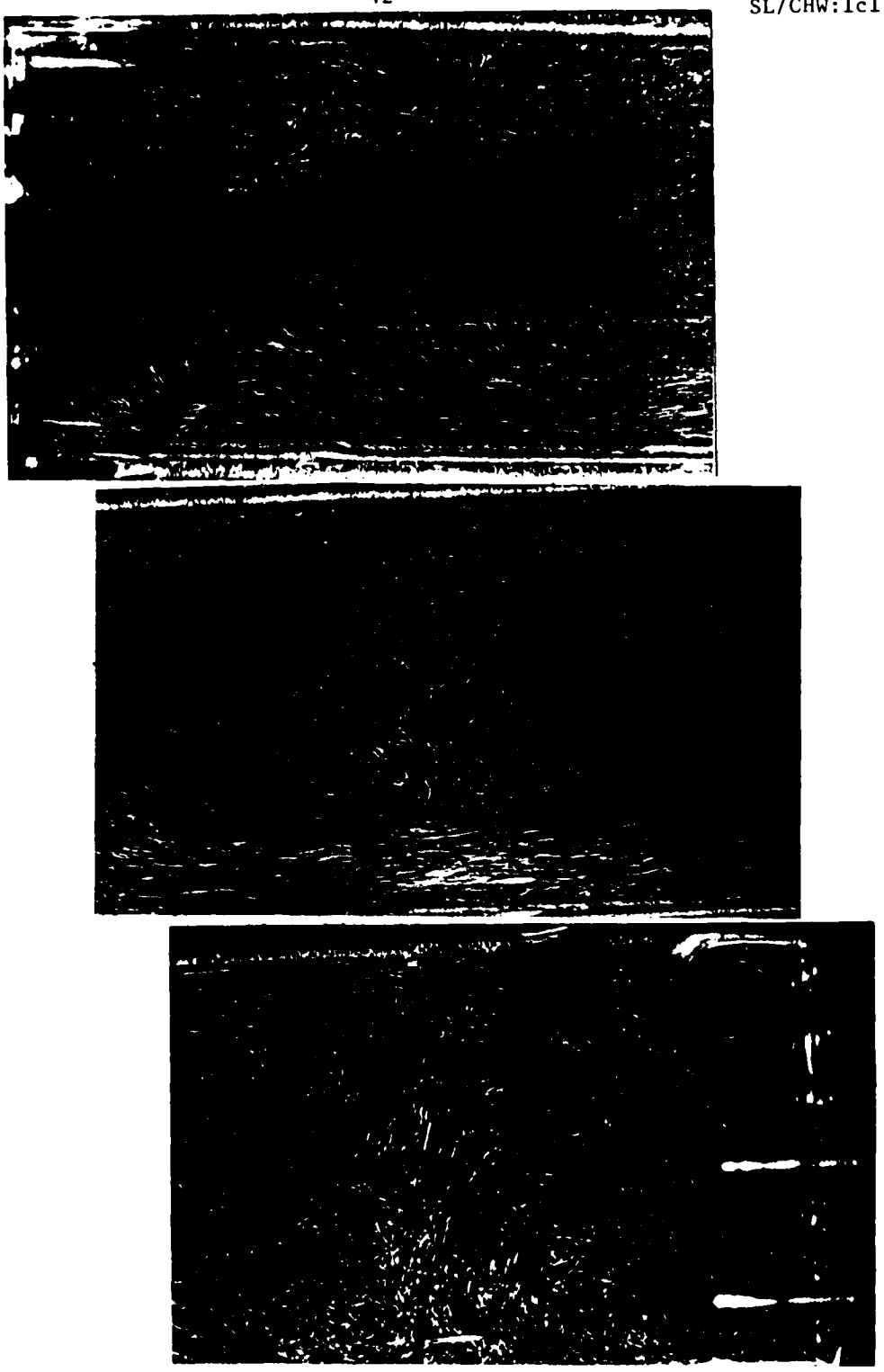

Fig. 16 Picture of Flow Field at Reynolds Number 32315

(outflow on injector end)

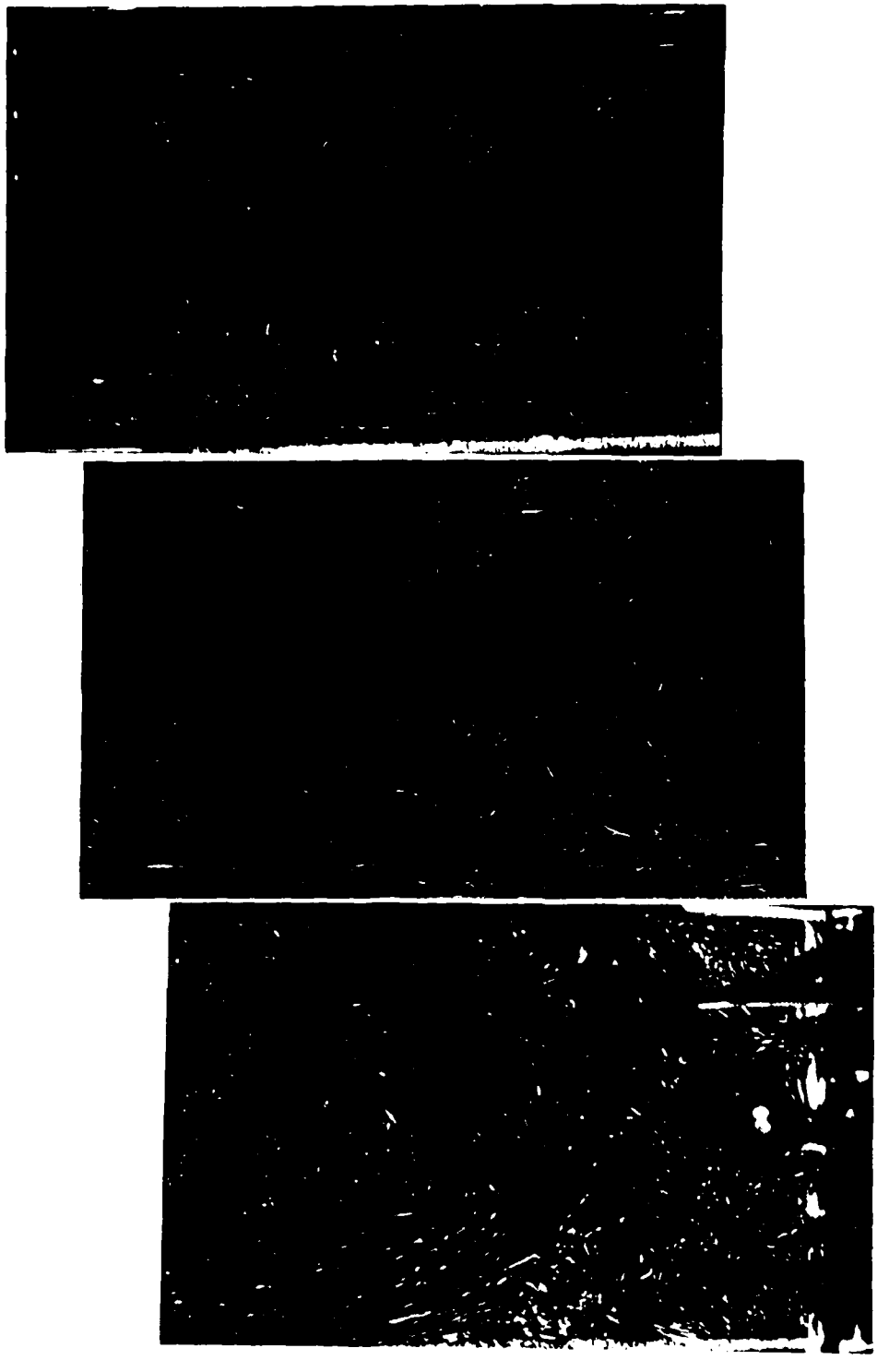

Fig. 17 Picture of Flow Field at Reynolds Number 18095

(outflow on injector end)

The outlet velocity profile was specified in two ways:

1. Assumed a specified uniform exit velocity profile.
2. Assumes a fully developed velocity profile at the exit plane.

Figure 18 shows that regardless of how the exit velocity profile is specified, the corresponding axial velocity profiles are within ±5% of each other at an x/L of just 0.065. As x/L increases the two profiles approach each other more closely. It is concluded that despite such big differences in the specified exit velocity profile, the downstream velocity profiles are not very different; the choice of outlet condition is not too important as long as continuity is satisfied. This comparison was made for a case with an injector diameter one third the size of the cylinder diameter, it is assumed that the same trend continues for smaller injector diameters, such as that in the model.

In all subsequent runs, a fully leveloped velocity profile was assumed at the exit plane. This provided for a more continuous variation in velocity profile from one axial location to the next.

Figure 19 shows the comparison between axial velocity profiles in the pipe step case and the modified case for the model.

The residues from iteration to iteration show good and stable convergence. The values of the residues for the U momentum, V momentum and continuity become very small, as does that for turbulent kinetic energy. The dissipation residue though small appears to be converging at a slower rate. These runs were made using the same under relaxation factors that were used in the original program. The values of the final

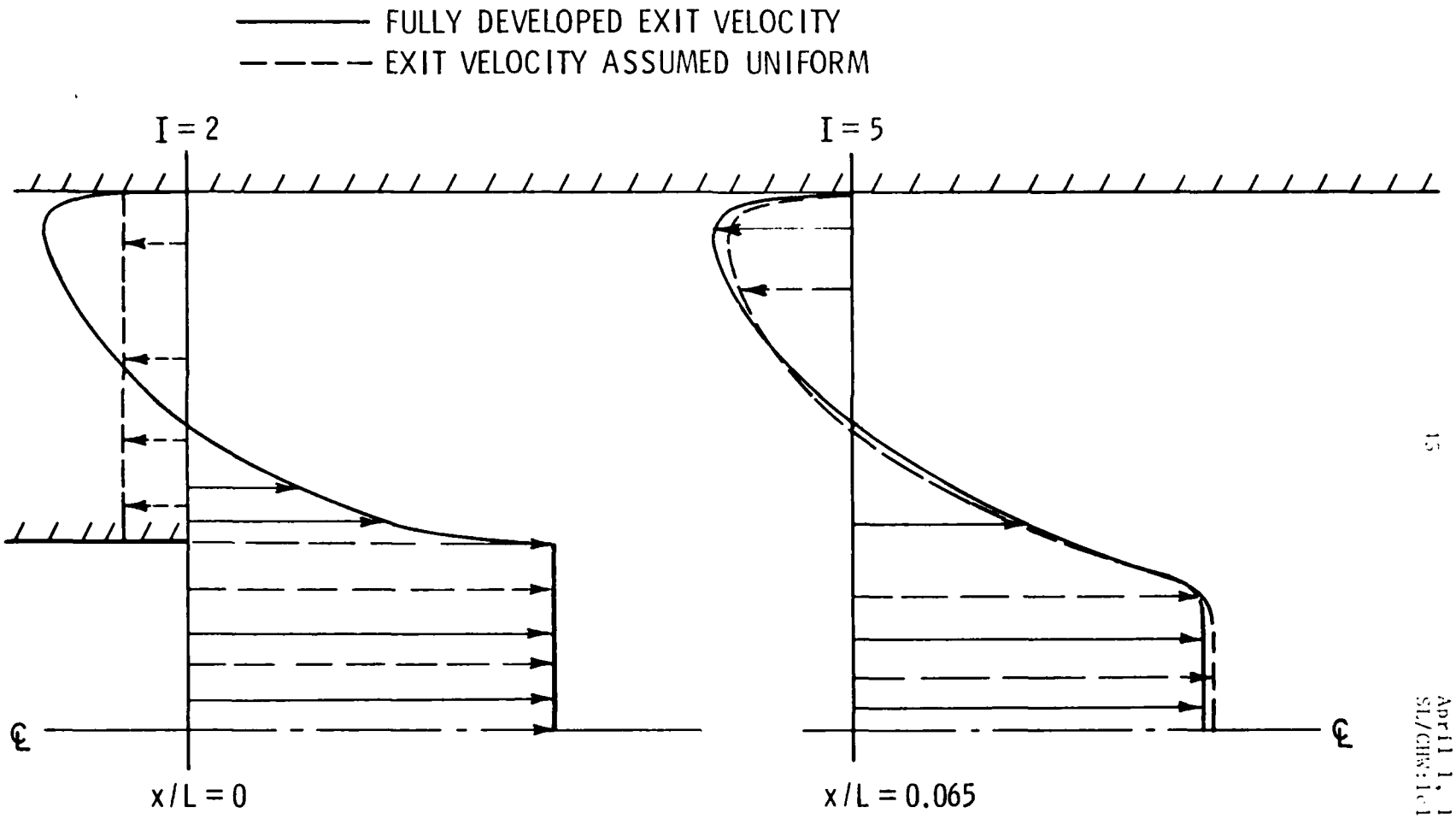

Fig. 15 Comparison of Axial Velocity Profiles Downstream of the Injector when using Different ways of Specifying the Outlet Condition.

April 1, 1980
SL/CBS:1c-1

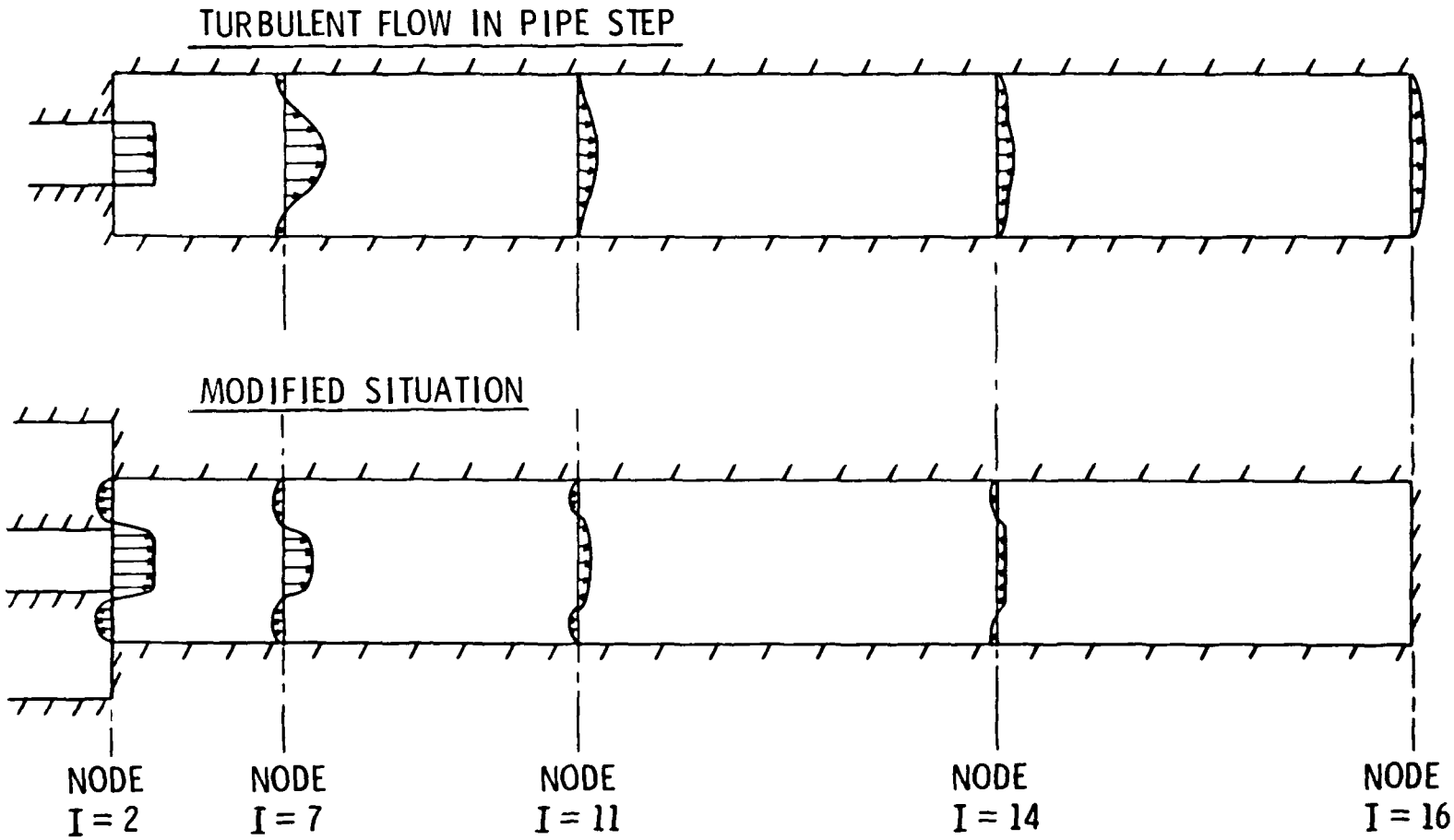

Fig. 19 Comparison of Axial Velocity Profiles at the Same Axial Locations for the Original TEACH Configuration and for the Modified Case.

April 1, 1980
SL/CHN:1c1

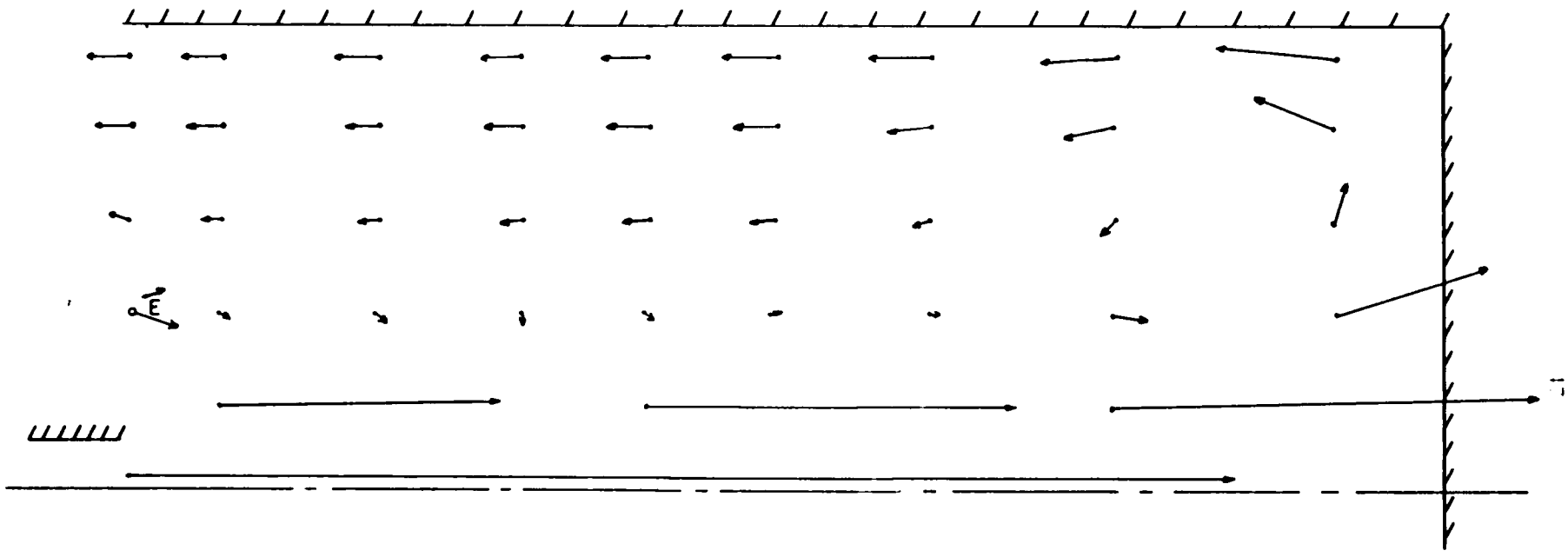

Fig. 20 Velocity Vectors at Selected Grid Points using Modified Computer Code

residues were only slightly higher than in the original test case.

Figure 20 shows the velocity vectors at some of the grid points for the case where the injector Reynolds number 25590, comparable to that of Figure 16. Appendix C tabulates data for this case. The figure shows a strong jet core with slight entrainment. The backflow is strong near the wall and eddies appear to exist, suc as in the stagnation region near the extreme end. Results obtained at both higher and lower Reynolds numbers show the same trend. Entrainment is very great in the injector vicinity as can be seen by the velocity vector $\bar{E}$ in Figure 20. Another interesting trend observed using the program at very high Reynolds number is the appearance of additional small eddies. It is important to realize that all eddies will not show up on the computer results since time averaging causes some of the regularly fluctuating eddies to disappear.

CHAPTER V

SUMMARY AND CONCLUSIONS

5.1 Summary

The objective of this study was to investigate the fluid flow structure of a jet induced mixing process in a SIR, where the jet is directed along the cylinder axis.

A water model was constructed which satisfied the conditions of similarity. The analogy leads to the conclusions that the flow pattern observed in the model is representative of that in the SIR and that the velocities in the model are related to those in the SIR.

The water model was a horizontal cylindrical vessel, containing a water bath at room temperature. A water jet was injected centrally from one end of the model and was continuously discharged through small holes on both ends. The water flowed in a closed loop for particle visualization studies and in an open loop for dye visualization. Runs were made at various inlet Reynolds numbers. The outflow on both ends was also varied.

Two techniques were used for the dye visualization studies in the model. Nozzle dye injection was employed to study the spreading behavior and the turbulent nature of the flow field. Syringe dye injection through glands in the model wall provided for a study of jet reattachment and eddy structure.

The particle visualization entailed photographing the generated flow patterns which were made visible by illuminating small alumina

particles placed in the water loop. The particles were visually observed in the model when they passed through a narrow zone of high intensity illumination. The narrow zone of light approximated a plane, containing the cylinder axis and point of injection.

A modified form of the TEACH computer code was used to make analytic predictions of velocity, pressure, turbulent kinetic energy, and dissipation fields in the specific case of a dead ended model with all outflow in the plane of injection.

5.2 Results and Conclusions

For a jet induced mixing process in a SIR, the major observations and conclusions of this investigation are:

1. The flow consisted of a spreading turbulent jet with a strong region of reverse flow near the walls. Eddy structure, predominant in the reverse flow region, indicated high turbulence intensity.
2. Fluctuating eddies caused the jet core flow to bend around them, producing a side to side whipping motion of the jet. The flow structure was highly fluctuating.
3. The jet did not reattach to the cylinder walls.
4. At high injector Reynolds numbers, the whipping was strong but confined to the extreme end of the model, where eddy structure was concentrated. The reverse flow along the wall was strong. Jet entrainment near the injector was high causing a rapid spreading.

For lower Reynolds numbers, the whipping motion was weak. Eddies were prevalent throughout the flow field causing a serpentine whipping. The reverse flow was weaker and the entrainment (hence spreading) less.

5. Outflow configuration was felt to have a major effect on the flow structure. The effect of higher outflow on the injector end was to produce higher reverse flow velocities near the walls, eddy structure became less prevalent, and a region of stagnation began to form at the extreme end. Increased outflow at the extreme end caused smaller reverse flow velocities, eddy structure became predominant especially in the central segment of the cylinder length, the stagnation region at the extreme end disappeared.
6. Results obtained using the modified form of TEACH are time averaged flow field variables, for a case with no outflow on the extreme end. Results showed a strong turbulent jet with a high velocity reverse flow. A stagnation region was encountered at the extreme end, where the streamlines of the jet bend into the region of reverse flow. Eddy structure was indicated.
7. Comparison between visual and analytic trends was not feasible. This was due to the fact that a time averaged visual structure could not be constructed.

5.3 Recommendations for Further Study

It would be of great value to record the flow patterns on movies or video tape. This would provide for a better understanding of the fluctuating structure and provide a base for time averaged visual observations.

Velocity measurements should be made to permit a thorough evaluation of the analytic model. The laser doppler velocimeter would seem to be the proper choice of instrument for such turbulent recirculating flow configurations.

The analytic model has potential for further modifications. It could be extended to account for outflow at both ends.

It is also suggested that a wider range of Reynolds number and length to diameter ratio be studied.

REFERENCES

1. Thomson, F. X., "Investigation of a Jet-Induced Mixing Heat Transfer Process," M.S. Thesis, The Pennsylvania State University, 1974.

2. Becker, H. A., Hottel, H. C. and Williams, G. C., "Mixing and Flow in Ducted Turbulent Jets," Ninth Symposium (International) on Combustion, Academic Press, London, 1963, pp. 7-20.

3. Barchion, M. and Curtet, R., "Some Details of the Structure of an Axisymmetric Confined Jet with Backflow," Transactions of the ASME, Journal of Basic Engineering, December 1964, pp. 777-787.

4. Craya, A. and Curtet, R., "On the Spreading of a Confined Jet," (in French) Comptes-rendus Academie des Sciences, Paris, Vol. 241, 1955, pp. 621-622.

5. Curtet, R., "Confined Jets and Recirculation Phenomena with Cold Air," Combustion and Flame, London, Vol. 2, No. 4, December 1958.

6. Curtet, R., "On the Flow of an Enclosed Jet," Publications Scientifiques et Techniques du Ministere de l'Air, Paris, No. 359, 1 60.

7. Abramovich, G. N., The Theory of Turbulent Jets, The M.I.T. Press, 1963.

8. Schlichting, H., Boundary Layer Theory, McGraw-Hill Co., 1968.

9. Hill, P. G., "Turbulent Jets in Ducted Streams," Journal of Fluid Mechanics, Vol. 22, Part 1, 1965, pp. 161-186.

10. Kerney, P. J., Faeth, G. M. and Olson, D. R., "Penetration Characteristics of a Submerged Steam Jet," AIChE Journal, Vol. 18, No. 3, 1972, pp. 548-554.

11. Weimer, J. C., Faeth, G. M. and Olson, D. R., "Penetration of Vapor Jets Submerged in Subcooled Liquids," AIChE Journal, Vol. 19, No. 3, 1973, pp. 552-557.

12. Avery, J. F. and Faeth, G. M., "Combustion of a Submerged Gaseous Oxidizer Jet in a Liquid Metal," Fifteenth Symposium (International) on Combustion, Academic Press, New York, 1974, pp. 501-512.

13. Gosman, A. D., Khalil, E. E. and Whitelaw, J. H., "The Calculation of Two-Dimensional Turbulent Recirculating Flows," First International Symposium on Turbulent Shear Flows, Springer-Verlat Berlin Heidelberg, 1979, pp. 237-255.

14. Gosman, A. D., Khalil, E. E. and Launder, B. E., "Computation of Flow in Ducts with Sudden Enlargements," Turbulent Recirculating Flows Workshop, The Pennsylvania State University, July 1975.

15. Launder, B. E. and Spalding, D. B., Mathematical Models of Turbulence, Academic Press, London, 1972.

16. Back, L. H. and Roschke, E. J., "Shear-Layer Flow Regimes and Wave Instabilities and Reattachment Lengths Downstream of an Abrupt Circular Channel Expansion," Journal of Applied Mechanics, Vol. 94, 1972, pp. 677-681.

17. Reynolds, A. J., "Observations of a liquid-liquid jet," Journal of Fluid Mechanics, Vol. 14, 1962, pp. 552-556.

18. McNaughton, K. H. and Sinclair, C. G., "Submerged Jets in Short Cylindrical Flow Vessels," Journal of Fluid Mechanics, Vol. 25, 1966, pp. 367-375.

19. Crow, S. C. and Champagne, F. H., "Orderly Structure in Jet Turbulence," Journal of Fluid Mechanics, Vol. 48, 1971, pp. 547-591.

20. White, W. N., Darooka, D. K. and Sogin, H. N., "On Recirculating Flow in a Dead-End Vessel," Transactions of the ASME, Journal of Fluids Engineering, March 1975, pp. 119-120.

21. Willis, D. A. and Meyer, W. E., "A Water Model Study of Swirling Flow in a Stratified Charge Engine," Department Report, Mechanical Engineering, The Pennsylvania State University, 1965.

22. Bird, R. B., Stewart, W. E. and Lightfoot, E. N., Transport Phenomena, John Wiley and Sons Inc., 2nd edition, 1962.

23. Prandtl, L. and Tietjen, O. J., Applied Hydro- and Aero-dynamics, Dover Publications Inc., 1957.

24. Ekchian, A. and Hoult, D. P., "Flow Visualization Study of the Intake Process of an Internal Combustion Engine," SAE Technical Paper Series, Detroit, February 1979.

25. Allen, M. and Yerman, A. J., "Neutral Density Beads for Flow Visualization," Section 4, Symposium of Flow Visualization, Presentation Summaries, ASME Annual Meeting, Chapter 4, 1960.

26. Merzkirch, W., Flow Visualization, Academic Press, New York, 1974.

27. Wood, C. J., "Visualization of an Incompressible Wake with Base Bleed," Journal of Fluid Mechanics, Vol. 29, 1967, pp. 259-272.

28. Fulmer, R. D. and Wirtz, D. P., "Measurement of Individual Particle Velocities in Simulated Rocket Exhaust," AIAA Journal, Vol. 3, No. 8, 1965, pp. 1506-1508.

APPENDIX A

CALCULATION OF FINITE DIFFERENCE EQUATION

COEFFICIENTS FOR NEW SIDE WALL

Refer to Figure 21 for the nodal configuration at the introduced extreme end wall. The boomerangs show had data is stored.

Consider the node (15,J) where J can vary from 2 to 21, the flux term (general) is defined as;

$$j_e = \rho u|_e \phi_e - \Gamma_\phi \frac{\partial \phi}{\partial x}|_e$$

For the axial velocity momentum equation,

$$j_e = \rho u|_e u_e - \Gamma_{u_e} \frac{\partial u}{\partial x}|_e$$

since u_e is very small and negligible in the near wall region

$$j_e = 0, \text{ therefore } A_e^u = 0.$$

Similarily for the V momentum;

$$j_e = \rho u_e v_e - \Gamma_{v_e} \frac{\partial v}{\partial x}|_e = -\Gamma_v \frac{V_{wall} - V(15)}{\Delta x(15)}$$

$$= \frac{\Gamma_v}{\Delta x(15)} V(15)$$

therefore

$$A_e^v = 0, \text{ and } S_p' = S_p - \frac{\Gamma_v}{\Delta x}$$

these changes in the source term S_p are made in accordance with the law of the wall, as used in the original program. Similar treatment is used for $\phi = k, \varepsilon$.

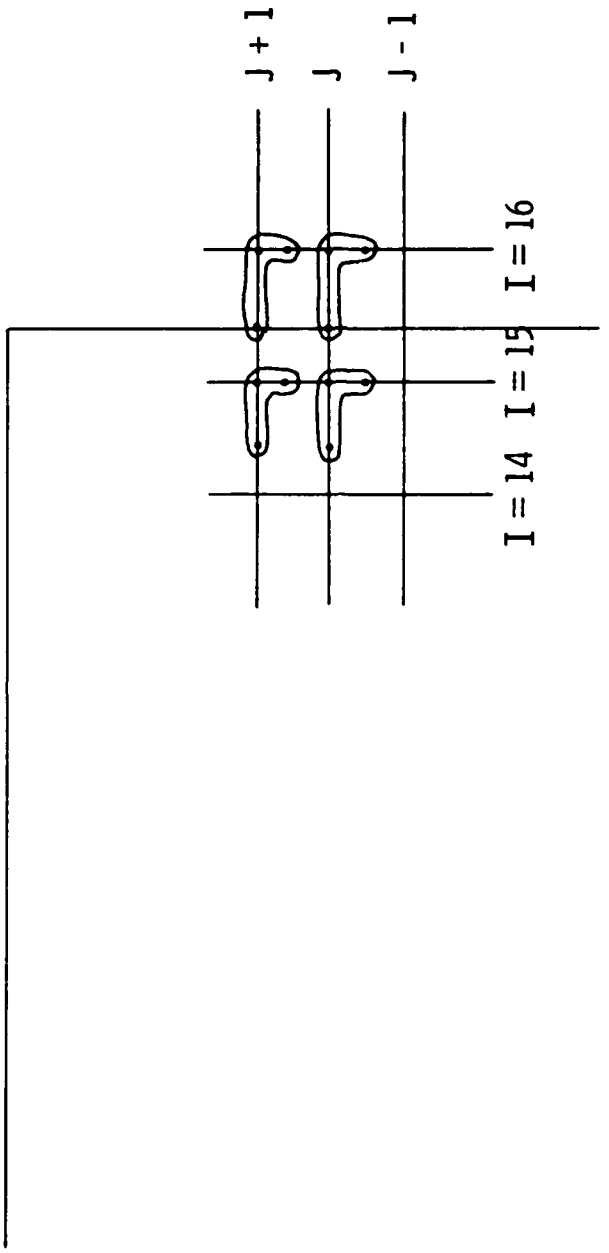

Fig. 21 Nodal Configuration at the Xes Side Wall (extreme end)

APPENDIX B

MODIFICATIONS IN THE COMPUTER CODE

The following changes were made in the computer code:

Changes in the MAIN PROGRAM

CHAPTER I

new values were assigned in the following statements, as shown:

```
NJ = 22
RLARGE = 0.0445
ALTOL = 7.0 * RLARGE
```

Statements numbered 43 and 44 were removed
The following statements were added:

```
RAT = RSMALL/RLARGE
UOUT = -UIN*RAT**2/(1.0-RAT**2)
TEOUT = TURBIN* UOUT**2
EDOUT = TEOUT**1.5/(ALAMDA*RLARGE)
```

CHAPTER II

The following statements were included:

```
      DO 201 J = JSTP1, NJM1
      TE(1,J) = TEOUT
      U(2,J) = UOUT
201   ED(1,J) = EDOUT

      DO 205 I = 2, NIM1
205   YPLUSN(I) = 11.0
```

Statement number 117 was replaced by;

```
      DO 657 J = 2, JSTEP
```

Changes in SUBROUTINE PROMOD

```
      ENTRY MODU
      C -------TOP WALL
      No changes required.
      C------- SIDE WALL
      DO 213 J = 2,NJM1
213   AE(NIM1,J) = 0.0
      C ------ SYMMETRY AXIS
      No changes required.
      C ------- OUTLET
      ARDENT=0.0
      FLOW=0.0
      DO 204 J=JSTP1, NJM1
      ARDEN = 0.5*(DEN(2,J)+DEN(3,J))*R(J)*SNS(J)
      ARDENT = ARDENT + ARDEN
204   FLOW=FLOW + ARDEN*U(3,J)
      UINC = (FLOWIN + FLOW)/ARDENT
```

```
      DO 205 J-JSTP1,NJM1
205   U(2,J) - U(3,J) -UINC
      RETURN

      ENTRY MODV
      C ------ SIDE WALL
      CDTERM = CMU**0.25
      XP =XU(NI)-X(NIM1)
      I =NIM1
      DO 310 J=2,NJM1
      SQRTK=SQRT(0.5*(TE(I,J)+TE(I,J-1)))
      DENV= 0.5*(DEN(I,J)+DEN(I,J-1))
      XPLUSA= 0.5*(XPLUSE(J)+XPLUSE(J-1))
      IF (XPLUSA.LE.11.63)   GO TO 311
      TMULT-DENV*CDTERM*SQRTK*CAPPA/ALOG(ELOG*XPLUSA)
      GO TO 312
311   TMULT-VISCOS/XP
312   TAUE(J) =-TMULT*V(I,J)
310   AE(I,J)=0.0
      TAUE(1)-TAUE(2)
      TAUE(NJ)-TAUE(NJM1)
      C ------ TOP WALL
      No changes required.
      C ------ SYMMETRY AXIS
      No change required.
      RETURN

      ENTRY MODP
      RETURN

      ENTRY MODT
      RETURN

      ENTRY MODTE
      C ----- TOP WALL
      No changes required
      C ----- SIDE WALL
      XP=XU(NI)-X(NIM1)
      I=NIM1
      DO 620 J=2,NJM1
      DENV=DEN(I,J)
      SQRTK-SQRT(TE(I,J))
      VOL=R(J)*SNS(J)*SEW(I)
      XPLUSE(J)=DENV*SQRTK*CDTERM*XP/VISCOS
      GENCOU=0.58(ABS(TAUE(J+1)*V(I,J+1))+ABS(TAUE(J)*V(I,J)))/XP
      DVDX=((V(I,J)+V(I,J+1)+V(I+1,J)+V(I+1,J+1))/4.-(V(I,J)+V(I,J+1)
           +V(I-1,J)+V(I-1,J+1))/4.0)/SEW(I)
      GENRLS=GEN(I,J)-VIS(I,J)*DVDX**2
      GEN(I,J)=GENRLS+GENCOU
```

```
      IF(XPLUSE(J).LE.11.63) GO TO 621
      DITERM=DEN(I,J)*(CMU**0.75)*SQRTK*ALOG(ELOG*XPLUSE(J))/ (CAPPA*XP)
      GO TO 622
621   CONTINUE
      DITERM=DEN(I,J)*(CMU**0.75)*SQRTK*XPLUSE(J)/XP
622   CONTINUE
      SU(I,J)=SU(I,J+SUKD(I,J)+GEN(I,J)*VOL
      SP(I,J)=SP(I,J)+SPKD(I,J)-DITERM*VOL
620   AE(I,J)=0.0
      C ----- SYMMETRY AXIS
      No changes required
      RETURN

      ENTRY MODED
      C ----- TOP WALL
      No changes required
      C ----- SIDE WALL
      XP=XU(NI)-X(NIM1)
      I=NIM1
      TERM=(CMU**0.75)?(CAPPA*XP)
      NJM2=NJ-2
      DO 720 J=2,NJM2
      SU(I,J)=GREAT*TERM*TE(I,J)**1.5
720   SP(I,J)=-GREAT
      C ----- SYMMETRY AXIS
      No changes required.
      RETURN
      END
```

April 1, 1980
SL/CHW:lcl

APPENDIX C

AXIAL AND RADIAL VELOCITIES AS CALCULATED BY THE MODIFIED TEACH PROGRAM CORRESPONDING TO A REYNOLDS NUMBER OF 25590.

April 1, 1980
SL/CHW:lcl

TABLE I

AXIAL VELOCITIES AT GRID POINTS AS CALCULATED BY MODIFIED TEACH

I / J	2	3	4	5	6	7	8
22	0.0	0.0	0.0	0.0	0.0	0.0	0.0
21	-4.25E-01	-4.02E-01	-3.98E-01	-3.95E-01	-3.95E-01	-3.99E-01	-4.08E-01
20	-4.25E-01	-4.20E-01	-4.15E-01	-4.11E-01	-4.08E-01	-4.09E-01	-4.14E-01
19	-4.19E-01	-4.14E-01	-4.09E-01	-4.04E-01	-4.01E-01	-4.01E-01	-4.05E-01
18	-4.00E-01	-3.96E-01	-3.92E-01	-3.88E-01	-3.85E-01	-3.85E-01	-3.88E-01
17	-3.72E-01	-3.69E-01	-3.66E-01	-3.63E-01	-3.61E-01	-3.62E-01	-3.62E-01
16	-3.35E-01	-3.33E-01	-3.32E-01	-3.31E-01	-3.31E-01	-3.32E-01	-3.35E-01
15	-2.90E-01	-2.91E-01	-2.92E-01	-2.93E-01	-2.95E-01	-2.97E-01	-3.01E-01
14	-2.40E-01	-2.43E-01	-2.47E-01	-2.50E-01	-2.54E-01	-2.58E-01	-2.63E-01
13	-1.87E-01	-1.92E-01	-1.98E-01	-2.03E-01	-2.08E-01	-2.15E-01	-2.22E-01
12	-1.33E-01	-1.40E-01	-1.47E-01	-1.52E-01	-1.59E-01	-1.68E-01	-1.78E-01
11	-8.21E-02	-8.93E-02	-9.34E-02	-9.76E-02	-1.06E-01	-1.18E-01	-1.31E-01
10	-2.25E-02	-2.25E-02	-3.10E-02	-3.56E-02	-4.56E-02	-6.01E-02	-7.56E-02
9	1.09E-01	9.92E-02	7.65E-02	5.36E-02	3.58E-02	1.89E-02	3.99E-03
8	2.45E-01	2.42E-01	2.30E-01	2.07E-01	1.82E-01	1.70E-01	1.73E-01
7	4.87E-01	4.88E-01	4.90E-01	4.97E-01	5.12E-01	5.44E-01	6.03E-01
6	1.05E+00	1.05E+00	1.07E+00	1.12E+00	1.19E+00	1.30E+00	1.42E+00
5	2.40E+00	2.40E+00	2.41E+00	2.44E+00	2.51E+00	2.62E+00	2.78E+00
4	5.50E+00	5.50E+00	5.49E+00	5.47E+00	5.43E+00	5.37E+00	5.31E+00
3	9.90E+00	9.90E+00	9.89E+00	9.88E+00	9.85E+00	9.79E+00	9.68E+00
2	9.90E+00	9.90E+00	9.90E+00	9.90E+00	9.90E+00	9.90E+00	9,90E+00
X =	0.0	0.006	0.012	0.02	0.029	0.040	0.054

TABLE I (cont.)

I / J	9	10	11	12	13	14	15	16
22	0.0	0.0	0.0	0.0	0.0	0.0	0.0	0.0
21	-4.23E-01	-4.64E-01	-4.79E-01	-5.29E-01	-6.07E-01	-7.67E-01	-1.17E+00	0.0
20	-4.24E-01	-4.41E-01	-4.66E-01	-5.04E-01	-5.62E-01	-6.97E-01	-1.08E+00	0.0
19	-4.13E=-1	-4.26E-01	-4.45E-01	-4.75E-01	-5.19E-01	-6.30E-01	-9.98E-01	0.0
18	-3.94E-01	-4.05E-01	-4.19E-01	-4.42E-01	-4.71E-01	-5.56E-01	-8.83E-01	0.0
17	-3.70E-01	-3.78E-01	-3.89E-01	-4.06E-01	-4.19E-01	-4.72E-01	-8.41E-01	0.0
16	-3.40E-01	-3.48E-01	-3.55E-01	-3.67E-01	-3.64E-01	-3.83E-01	-5.70E-01	0.0
15	-3.07E-01	-3.13E-01	-3.18E-01	-3.25E-01	-3.05E-01	-2.90E-01	-3.72E-01	0.0
14	-2.70E-01	-2.76E-01	-2.78E-01	-2.83E-01	-2.45E-01	-1.98E-01	-1.47E-01	0.0
13	-2.30E-01	-2.36E-01	-2.36E-01	-2.40E-01	-1.84E-01	-1.08E-01	1.05E-01	0.0
12	-1.87E-01	-1.95E-01	-1.92E-01	-1.95E-01	-1.22E-01	-1.87E-02	3.81E-01	0.0
11	-1.42E-01	-1.50E-01	-1.43E-01	-1.45E-01	-5.57E-02	7.18E-02	6.48E-01	0.0
10	-8.77E-02	-9.52E-02	-8.55E-02	-7.58E-02	5.20E-02	1.72E-01	1.02E+00	0.0
9	-3.92E-03	-1.74E-03	2.52E-02	6.67E-02	1.72E-01	3.06E-01	1.39E+00	0.
8	1.94E-01	2.40E-01	2.91E-01	4.21E-01	4.68E-01	5.45E-01	1.82E+00	0.0
7	6.88E-01	8.03E-01	9.08E-01	1.10E+00	1.08E+00	1.09E+00	2.31E+00	0.0
6	1.58E+00	1.74E+00	1.89E+00	2.09E+00	2.07E+00	2.28E+00	2.89E+00	0.0
5	2.95E+00	3.13E+00	3.28E+00	3.43E+00	3.42E+00	3.85E+00	3.55E+00	0.0
4	5.26E+00	5.25E+00	5.26E+00	5.29E+00	5.24E+00	5.66E+00	4.25E+00	0.0
3	9.49E+00	9.23E+00	8.91E+00	8.54E+00	8.13E+00	8.10E+00	4.94E+00	0.0
2	9.90E+00	9.88E+00	9.85E+00	9.77E+00	9.63E+00	9.57E+00	5.39E+00	0.0
X =	0.069	0.089	0.112	0.139	0.172	0.212	0.260	0.31

April 1, 1980
SL/CHW:lcl

TABLE II

RADIAL VELOCITIES AT GRID POINTS AS CALCULATED BY MODIFIED TEACH

I / J	2	3	4	5	6	7	8
22	0.0	0.0	0.0	0.0	0.0	0.0	0.0
21	1.36E-03	1.19E-03	7.17E-04	4.15E-05	-7.18E-04	-1.50E-03	-2.20E-03
20	3.25E-03	3.12E-03	2.04E-03	6.39E-04	-8.97E-04	-2.45E-03	-3.84E-03
19	5.26E-03	5.23E-03	3.49E-03	1.38E-03	-9.02E-04	-3.19E-03	-5.22E-03
18	7.16E-03	7.23E-03	4.84E-03	2.08E-03	-8.89E-04	-3.87E-03	-6.49E-03
17	8.79E-03	8.91E-03	5.93E-03	2.61E-03	-9.80E-04	-4.59E-03	-7.73E-03
16	9.97E-03	1.00E-02	6.58E-03	2.84E-03	-1.29E-03	-5.47E-03	-9.05E-03
15	1.06E-02	1.04E-02	6.69E-03	2.67E-03	-1.92E-03	-6.59E-03	-1.05E-02
14	1.04E-02	9.84E-03	6.20E-03	2.02E-03	-2.99E-03	-8.09E-03	-1.23E-02
13	9.28E-03	8.51E-03	5.21E-03	8.39E-04	-4.65E-03	-1.01E-02	-1.45E-02
12	7.46E-03	6.95E-03	4.08E-03	-8.85E-04	-7.04E-03	-1.29E-02	-1.73E-02
11	5.31E-03	6.18E-03	3.24E-03	-3.13E-03	-1.04E-02	-1.66E-02	-2.08E-02
10	3.13E-03	6.23E-03	2.19E-03	-6.13E-03	-1.48E-02	-2.14E-02	-2.52E-02
9	-4.25E-04	-1.42E-03	-4.65E-03	-1.16E-02	-2.05E-02	-2.72E-02	-3.00E-02
8	-1.76E-03	-6.13E-03	-1.28E-02	-2.00E-02	-2.67E-02	-3.11E-02	-3.19E-02
7	-1.77E-03	-6.56E-03	-1.33E-02	-2.01E-02	-2.48E-02	-2.66E-02	-2.53E-02
6	2.09E-04	-6.56E-05	-1.74E-03	-4.87E-03	-7.95E-03	-9.09E-03	-7.94E-03
5	8.45E-04	3.47E-03	7.29E-03	1.20E-02	1.61E-02	1.82E-02	1.80E-02
4	1.47E-03	1.72E-03	2.54E-03	4.81E-03	8.95E-03	1.45E-02	1.97E-02
3	3.35E-05	1.59E-04	1.11E-04	2.41E-05	-3.78E-05	-1.08E-05	1.96E-04
2	0.0	0.0	0.0	0.0	0.0	0.0	0.0
X =	0.003	0.009	0.016	0.024	0.034	0.046	0.061

TABLE II (cont.)

I / J	9	10	11	12	13	14	15	16
22	0.0	0.0	0.0	0.0	0.0	0.0	0.0	0.0
21	-2.77E-03	-3.25E-03	-4.10E-03	-5.34E-03	-9.21E-03	-1.93E-02	5.14E-02	0.0
20	-4.94E-03	-5.84E-03	-7.46E-03	-9.67E-03	-1.75E-02	-3.89E-02	1.02E-01	0.0
19	-6.28E-03	-8.07E-03	-1.04E-02	-1.33E-02	-2.50E-02	-5.88E-02	1.52E-01	0.0
18	-8.51E-03	-1.00E-02	-1.30E-02	-1.61E-02	-3.14E-02	-7.83E-02	2.00E-01	0.0
17	-1.01E-02	-1.18E-02	-1.52E-02	-1.81E-02	-3.66E-02	-9.65E-02	2.46E-01	0.0
16	-1.17E-02	-1.34E-02	-1.73E-02	-1.91E-02	-4.03E-02	-1.12E-01	2.89E-01	0.0
15	-1.34E-02	-1.49E-02	-1.92E-02	-1.92E-02	-4.25E-02	-1.25E-01	3.28E-01	0.0
14	-1.52E-02	-1.63E-02	-2.13E-02	-1.82E-02	-4.33E-02	-1.33E-01	3.62E-01	0.0
13	-1.74E-02	-1.78E-02	-2.35E-02	-1.59E-02	-4.27E-02	-1.35E-01	3.90E-01	0.0
12	-2.00E-02	-1.94E-02	-2.60E-02	-1.23E-02	-4.10E-02	-1.29E-01	4.12E-01	0.0
11	-2.32E-02	-2.90E-02	-2.90E-02	-7.20E-03	-3.81E-02	-1.13E-01	4.27E-01	0.0
10	-2.70E-02	-2.23E-02	-3.20E-02	-3.90E-04	-3.45E-02	-8.47E-02	4.34E-01	0.0
9	-3.06E-02	-2.29E-02	-3.28E-02	7.15E-02	-3.14E-02	-4.26E-02	4.32E-01	0.0
8	-3.00E-02	-2.14E-02	-2.68E-02	1.17E-02	-3.19E-02	1.47E-02	4.20E-01	0.0
7	-2.13E-02	-1.44E-02	-1.49E-02	1.25E-02	-3.77E-02	8.03E-02	3.96E-01	0.0
6	-4.97E-03	-1.42E-03	-7.78E-04	1.44E-02	-3.43E-02	1.33E-01	3.55E-01	0.0
5	1.68E-02	1.52E-02	1.35E-02	1.86E-02	-1.81E-02	1.61E-01	2.96E-01	0.0
4	2.32E-02	2.41E-02	2.35E-02	2.34E-02	2.03E-03	1.59E-01	2.17E-01	0.0
3	7.16E-04	1.58E-03	3.09E-03	4.77E-03	1.85E-03	9.75E-02	1.15E-01	0.0
2	0.0	0.0	0.0	0.0	0.0	0.0	0.0	0.0
X =	0.078	0.099	0.124	0.154	0.190	0.234	0.286	0.33

DISTRIBUTION LIST - TM 80-46

NAVSEA, Mr. M. F. Murphy, SEA 63R-32, Copy No. 1
NAVSEA, Mr. F. J. Romano, SEA 63R-3, Copy No. 2
NAVSEA, Mr. C. D. Smith, SEA 63R, Copy No. 3
NAVSEA, Library, SEA-9961, Copies No. 4 and 5
NUSC, Dr. R. S. Lazar,3642, Copy No. 6
NUSC, Mr. T. J. Black, Copy No. 7
DTIC, Copies 8 through 19